공학박사학위논문

Analysis on Membrane Electrode Assembly for Intermediate Temperature Proton Exchange Membrane Fuel Cell and Alkaline Anion Exchange Membrane Water Electrolysis

중온 양이온 교환막 연료전지와 알칼리 음이온 교환막 수전해 장치용 막-전극 접합체 연구

2017년 02월

서울대학교 대학원

화학생물공학부

조민경

Abstract

Analysis on Membrane Electrode Assembly for Intermediate Temperature Proton Exchange Membrane Fuel Cell and Alkaline Anion Exchange Membrane water Electrolysis

Min Kyung Cho

School of Chemical and Biological Engineering

The Graduate School of Engineering

Seoul National University

With the increase in interest of hydrogen energy as an alternative energy source, the research on electrochemical devices to generate electricity using hydrogen as fuel and to produce hydrogen using water as reactant are actively pursued. Proton exchange membrane fuel cells are electrochemical devices that convert hydrogen and oxygen to electricity and water. The higher thermodynamic efficiency (> 40%) than conventional internal combustion engines (20 – 30%) and no greenhouse gas emission during operation are the great advantages of the proton

exchange membrane fuel cells. The hydrogen production is dominantly performed through steam reforming from natural gas or methane, which process creates carbon dioxide or hydrocarbons as byproducts. Water electrolysis is a technique that decomposes water into oxygen and hydrogen gas only through electrochemical reaction. This technique primarily using renewable power sources and make it possible to yield high purity hydrogen without greenhouse gas emission. To establish green technology system from hydrogen production to converting hydrogen into electricity, the intensive research on developing fuel cell and water electrolysis technology are conducted.

The intermediate-temperature proton exchange membrane fuel cells are operating at higher temperature (100–120 °C) than low-temperature proton exchange membrane fuel cells (~ 80 ºC). The higher operating temperature of the system improves the reaction kinetics, CO tolerance and heat/water management. Therefore, many advantages are expected with proton exchange membrane fuel cells operating at intermediate temperature compared to that at low temperature. Alkaline anion exchange membrane water electrolysis has advantages over the conventional alkaline water electrolysis that uses alkaline solution electrolyte with porous diaphragm separators. The polymer electrolyte membrane based systems offer advantages with regard to safety, efficiency, and separation of product gases. Moreover, the alkaline operating condition makes it possible to use inexpensive non-noble metal catalysts towards oxygen evolution and hydrogen evolution reaction unlike in proton exchange membrane water electrolysis. Even though with

these great advantages, intermediate temperature proton exchange membrane fuel cells or alkaline anion exchange membrane water electrolysis show relatively low performances than low temperature proton exchange membrane fuel cells or proton exchange membrane water electrolysis, respectively due to their operational characteristics. To overcome this issue and obtain high performance and durability, the research on developing polymer electrolyte and catalysts are actively conducted.

Most of the researches are oriented to the material development. Even though the developed polymer electrolyte or catalysts showed great material property, their performances are not reflected in a cell performance. A single cell is containing a membrane electrode assembly which is consisted with a polymer electrolyte membrane and catalyst layer on both side of the membrane. The catalyst layer, which consists of the metal catalysts and binders, is an important component of the membrane electrode assemblies since the electrochemical reactions are occurred in there involving mass transport of reactants and products. Therefore, the catalyst layer structure and properties should be optimized regarding on each operating condition of the electrochemical devices to obtain high performance and stability. For intermediate temperature proton exchange membrane fuel cell operation, membrane electrode assembly drying is a dominant factor influencing the cell performance since the ionic conductivity and mass transport of the catalyst layer are strongly dependent on the ionomer films layered on the catalyst particles. In the research of intermediate temperature proton exchange membrane fuel cell, the drying of electrode membrane electrode assembly at 120 ^{o}C and $\leq$ 35% RH

operating condition is experimentally proven and the contents of ionomeric binder, which has water retention ability, is controlled to 20 – 40 wt.% to construct effective catalyst layers for high performance. The optimum ionomer content increases with decreasing current density where the drying of membrane electrode assembly is dominant over flooding. However, at high current density region where the water production is high and sufficient hydration is provided, the maximum performance is obtained with 30 wt% ionomer content due to flooding. For alkaline anion exchange membrane water electrolysis operation, the effect of pressing of membrane electrode assembly and feed supplying methods are investigated. Through introducing pressing procedure, higher water splitting current density is obtained due to the improvement is mass transport. Additionally, the characteristics of double-side feed (supplying reactant solutions to both anode and cathode) and single-side feed operation (supplying a reactant solution to only anode) are studied with various anode binder content. In double-side feed operating condition, the cell performance is dominantly affected by electrochemical activation site of the catalyst and porosity of the catalyst layers. The optimal content is found to be 9 wt.% between 5 – 20 wt.%. In single-side operating condition, the water splitting current density has been greatly increased by improvement in mass transport and catalyst dissolution during the cell operation due to the high water splitting current resulted in massive oxygen production dominantly affects the long-term performance stability. Therefore, the highest binder content in this experiment, 20 wt.%, exhibits the best durability and cell performance. In this study, the electrochemical factors affecting cell performances are analyzed and research directions of membrane

electrode assembly for high performance are proposed regarding on the operating conditions of electrochemical devices.

***Keywords*:** Membrane Electrode Assembly, Binder Content, Intermediate Temperature Proton Exchange Membrane Fuel Cells, Alkaline Anion Exchange Membrane Water Electrolysis, Electrochemistry

***Students Number*:** 2012-31302

Contents

List of Figures

Chapter 1. Introduction

1.1 Hydrogen Energy

The emission of greenhouse gases, mainly from the combustion of fossil fuels, has become a serious issue while global energy consumption is rapidly increasing [1, 2]. The accumulated carbon dioxide in the atmosphere is considered the main cause of global warming and climate change [3, 4]. To mitigate the environmental impact of greenhouse gases by reducing the use of fossil fuels, alternative energy has been actively pursued for decades [5-10]. Among the various energy carriers, hydrogen is not only abundant, but also has high mass energy density (39.4 kWh/kg) [11] and high energy efficiency (> 70%) [12]. As research towards hydrogen energy increases, the development of fuel cell technology also attracts much attention as a promising technology. Fuel cells are electrochemical devices that produce electricity and water from hydrogen as a fuel source. Fuel cells are generally categorized regarding on the electrolytes employed in the systems which are proton exchange membrane/polymer electrolyte membrane fuel cells, alkaline fuel cells, phosphoric acid fuel cells, molten carbonate fuel cells and solid oxide fuel cells. Their operation temperatures are varied from 50 to 1000 ^{o}C regarding on the thermal property of electrolytes used. Amongst them, proton exchange membrane fuel cells have advantages in fast start up from low working temperature, safety from the use of solid electrolyte membrane and compact

constructions which make the fuel cells possible to use in the applications for vehicle, public transportation or portable power generation [13].

Hydrogen is currently produced mainly by steam reforming of natural gas, a process that creates carbon dioxide or hydrocarbons as byproducts. Therefore, cleaner alternatives such as water electrolysis, water gasification, and photolysis are needed [14-19]. Water electrolysis has advantages over other hydrogen production technologies, primarily by using renewable power sources (e.g., wind, geothermal, or solar energy) to yield high-purity hydrogen without greenhouse gas emission. Water electrolysis is a well-known principle to produce hydrogen and oxygen by decomposing water. It is discovered by William William Nicholson and Anthony Carlisle in 1800's and started to use in industrial field. The pressurized system of industrial electrolyzer was developed by Zdansky/Lonza in 1948 and made it possible to have massive hydrogen production with improvement in hydrogen storage and transportation systems [20]. The electrochemical water electrolysis cell is containing pure water and has two electrodes connected to an external power supply. The gas production rate is controlled by the current applied into the cell, and oxygen and hydrogen are produced at anode and cathode electrode, respectively. Additionally, on-site fueling stations for water electrolysis require relatively less space due to the low operating temperature, and they could also use the existing water and electricity infrastructure [12].

Both fuel cells and water electrolysis systems have a solid polymer membrane based technology to generate electricity from hydrogen or to generate

hydrogen from water. The solid polymer membrane based cell systems are consisted with membrane electrode assembly, diffusion layers, flow field plates and end plates as shown in Fig. 1.1. Membrane electrode assembly is composed of ion conducting membrane with catalyst layers, which is the mixture of catalysts and ionomer or binder [21]. Diffusion layers allow the flow of reactants and products to or from the membrane electrode assembly. They are electrical conductors to deliver electrons to or from the catalyst to the flow field plates [22]. Flow field plates supply fuel, remove products and work as a current collector [23]. End plates provides uniform pressure between the single cell components to reduce contact resistance between them [24]. Within the membrane electrode assembly, reactants are transferred from diffusion layers to the catalysts through the pores of catalyst layer. Ions are transferred through the membranes and electrons are transported though the catalyst, to the diffusion layer and to the current collector to fulfill the required reactions. As the heart of the electrochemical device systems where the electrochemical reaction is occurred, the optimization of membrane electrode assembly is desired to obtain high cell performance.

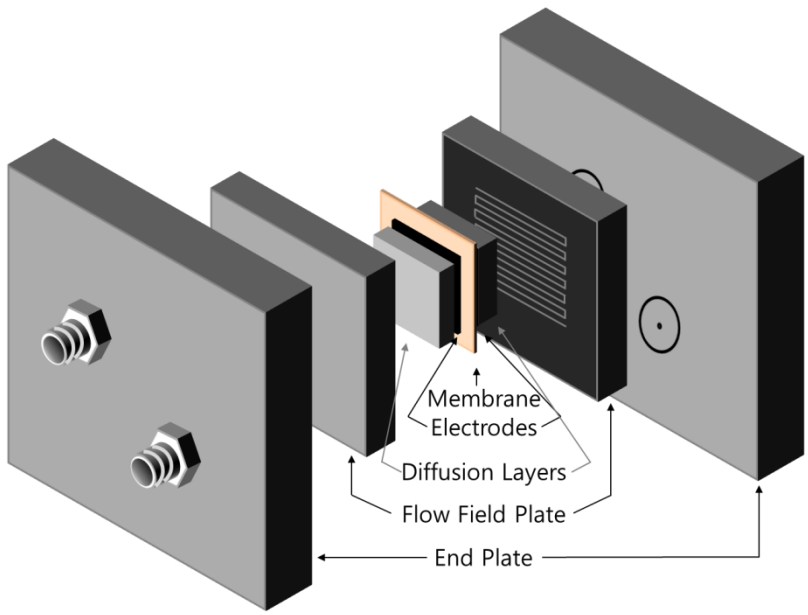

Figure 1.1. Configuration of a single cell

1.2. Intermediate Temperature Proton Exchange Membrane Fuel Cell (IT-PEMFC)

Polymer electrolyte membrane fuel cells (PEMFCs) have been extensively studied as efficient energy conversion devices utilizing gaseous hydrogen and oxygen to generate electricity [25-27] as presented in Fig. 1.2. Since the electrochemical conversion of chemical energy to electric energy provides significantly higher thermodynamic efficiency (> 40%) than conventional internal combustion engines (20–30%), various types of PEMFCs have been investigated, including those operated at low (~80 °C), intermediate (100 – 120 °C), and high temperatures (up to 200 °C) for practical PEMFC deployment [2]. Among the different PEMFCs studied, intermediate-temperature PEMFCs (IT-PEMFCs) [25] have received much attention due to their superior heat/water management, CO tolerance, and electrode reaction kinetics [26, 27] than the low temperature (LT-) PEMFCs. However, the reliability and performance of IT-PEMFCs should be further enhanced to be utilized commercially as portable and stationary power sources. Due to the poor thermal stability at a glass transition temperature < 110 °C [28], the commercial perfluorosulfonic acid polymers with long side chains, such as Nafion®, which is commonly used in the low temperature PEMFC, cannot be applied in IT-PEMFC. Moreover, the dehydrated operating conditions requires higher conductivity of materials to maintain sufficient proton conductivity along with high thermal stability.

An IT-PEMFC employs a membrane electrode assembly (MEA), composed of anode and cathode catalyst layers, a polymer membrane electrolyte, and gas diffusion layers to conduct the electrochemical redox reactions with appropriate electronic and ionic conductivities and molecular mass transport. Several polymer membrane electrolytes have been reported, e.g. short-side-chain perfluorinated sulfonic acid (SSC PFSA) [29-31], sulfonated hydrocarbon polymer [32-35], polymer/inorganic composites [36-39], etc. The PFSA polymers with long side chains, such as Nafion®, are conventionally used in LT-PEMFCs (60 – 80 °C) [40], but they do not have stable function in IT-PEMFCs due to poor thermal stability at a glass transition temperature < 110 °C [28].

The catalyst layer, which consists of the metal catalysts and the ionic conductors, is a key component of PEMFC MEAs. Since the hydrogen oxidation reaction (HOR) and the oxygen reduction reaction (ORR) essentially occur in the catalyst layer, involving mass transport of reactants and products, the catalyst layer structure and properties should be optimized to achieve high PEMFC performance and stability. Therefore, the catalyst layer structure in LT-PEMFCs have been intensively researched for decades, focusing on various variables, including ionomer content [41-46], catalyst loading [47], catalyst layer structure [45, 48-50] and thickness of catalyst layer[51]. Especially, the optimum ionomer loading and the resultant microstructure should be determined in terms of the preparation methods, catalyst, and ionomer materials under desired cell operating conditions. Generally, proton conductivity in catalyst layers increases with increasing ionomer

loading; however, water removal rate decreases simultaneously, leading to significant flooding. As the proton conduction and water removal characteristics are strongly dependent on the operating conditions, such as relative humidity (RH) and current density, the optimum ionomer loading should be discussed for specific operating conditions.

Under the elevated operating temperature with the supply of low relative humidified gases, drying become dominant and the poor ion conductivity affects the performance degradation. Since the ionic conductivity and mass transport of the catalyst layer are strongly dependent on the ionomer films layered on the catalyst particles, the efficient operation of IT-PEMFC under extremely low humidification conditions would be significantly affected by the properties of the ionomer in the catalyst layer. Briefly, the amount of ionomer present in the catalyst layer should produce sufficient ionic conductivity to minimize the ohmic drop under dried conditions, whereas mass transport can be hindered if excess ionomer and water are present in the electrodes. Especially under dehydrated operating conditions, the higher ionomer content can be advantageous because it can retain water molecules, resulting in better performance with increased ionic conductivity. Hydration of the MEA is further affected by other electrode properties, e.g. porosity, hydrophobicity, thickness, etc. and by operation conditions, e.g. RH, applied current, reactant flow rates, temperature, etc. [52, 53]. Therefore, effective

catalyst layers with optimum ionomer content should be designed to obtain highest IT-PEMFC performance under specific operating conditions.

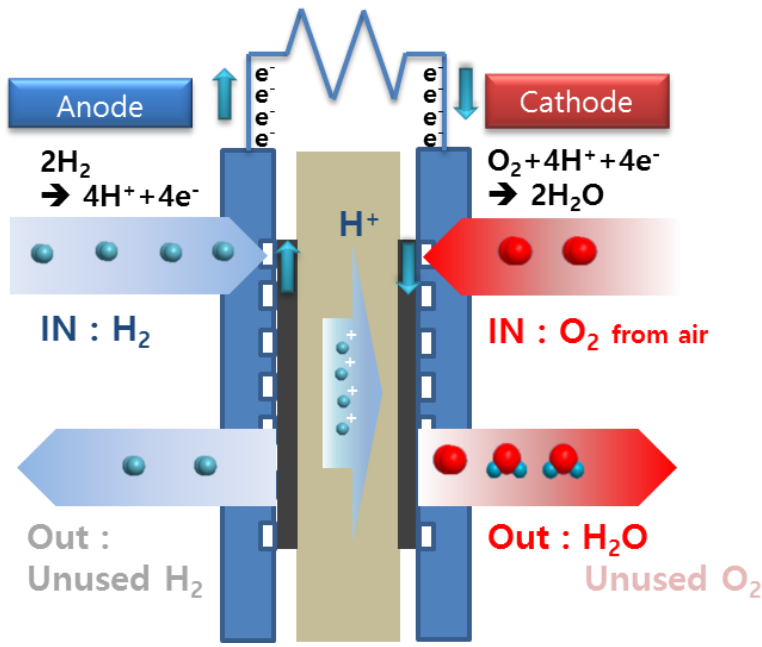

Figure 1.2. Schematic of PEMFC single cell

1.3. Hydrogen Production by Alkaline Anion Exchange Membrane Based Water Electrolysis (AEMWE)

Recently, water electrolysis using a solid polymer electrolyte membrane has been intensively investigated [54, 55]. Compared to conventional alkaline water electrolysis that uses alkaline solution electrolytes with porous diaphragm separator (Fig. 1.3.), the polymer electrolyte membrane-based systems (Fig. 1.3.) offer advantages with regard to safety, efficiency, and separation of the product gases [56]. Two kinds of solid polymer electrolytes are used: proton exchange membranes (PEMs) [57] and alkaline anion exchange membranes (AEMs) [58]. PEM-based water electrolysis (PEMWE) has shown high performance in producing hydrogen without emitting pollutants. However, it requires acid-resistant noble metal catalysts, e.g., platinum, and expensive perfluorinated membranes such as Nafion® in the water splitting device [56, 59]. On the other hand, as AEMWE systems are operated under high pH, inexpensive non-noble metal electrocatalysts can be utilized towards oxygen evolution and hydrogen evolution reactions [60]. Therefore, AEMWE should resolve the cost issue of the PEMWE system while satisfying the environmental requirements.

However, the water splitting performance of AEMWE is currently much lower than that of PEMWE due to the slower mobility of OH^- ions compared to H^+ ions in aqueous solution [61]. Hence, performance enhancement through new

materials and membrane electrode assemblies (MEAs) are highly desirable. There have been many studies to develop AEMs with high ionic conductivity and stability [62-77], as well as catalysts with improved activity and durability in alkaline conditions [78-81]. Moreover, the optimization of electrode/MEA fabrication is also very essential for improving the performance and durability of electrochemical devices [82-86]. Nevertheless, only a few studies have examined the effects of relevant factors, such as catalyst loading [87], hydroxide ion-conducting inorganic binder with pore formers [88], and electrodeposited low-loading electrodes [89]. Therefore, further optimization of MEA fabrication methods is urgently needed.

In this study, high performance MEAs were fabricated through investigating the effects of MEA pressing conditions and catalyst layer structure. The studies on reaction kinetics and mass transport were also conducted with varying the feed configuration. The characteristics of MEA performance and performance influencing factors were analyzed through electrochemical analyses.

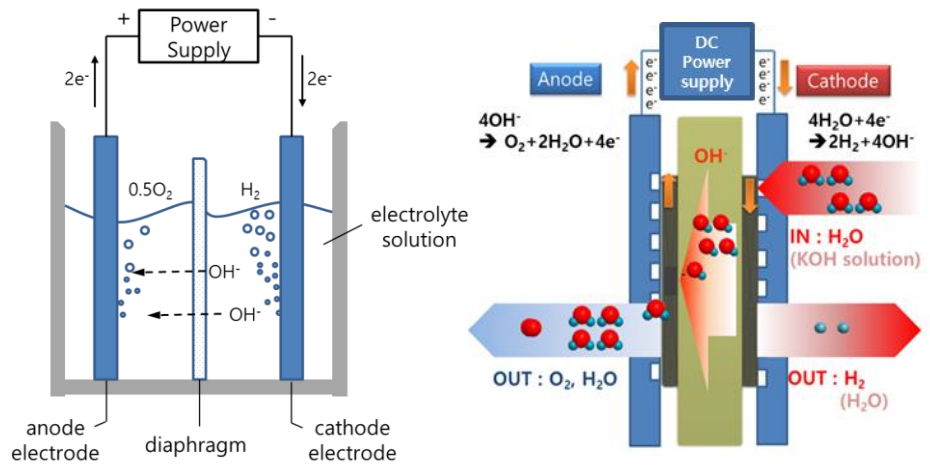

Figure 1.3. Schematic of alkaline water electrolysis with porous diaphragm separator (left) and that of alkaline anion exchange membrane water electrolysis (AEMWE) with anion conducting solid polymer electrolyte membrane (right).

1.4. Research Objective

An MEA of a single cell is one of the key components in the cell operation. There are many studies on developing catalysts with higher activity than the commercially available platinum group metal catalysts while reducing the cost of the materials [90]. However, the great advantages of the developed catalysts are not reflected in the performance of the MEA. Therefore, the optimization of catalyst layer is required to maximize the performance of MEA fabricated with the developed catalysts. Through the optimization of catalyst layers by controlling the microstructure, the relevant reactions are occurred efficiently within the MEA including the mass transport of reactant and products. High ionic conductivity with facile mass transport of reactant and products are important to achieve high performance. To maximize the cell performances, understanding the performance degradation mechanism and analyzing performance influencing factor by controlling the microstructure of catalyst layer and operating conditions are performed.

The objective of this research is to develop high performance MEAs for IT-PEMFCs and AEMWEs. In order to achieve the goal, performance dependence on structure change of catalyst layer and operating conditions are studied. Polarization overpotentials and electrochemical impedances are analyzed to find change in kinetics and mass transport with varying ionomer/binder content. The findings

from each application through the electrochemical analyses provide valuable insights on optimization of MEA to achieve high efficiency of the system.

The dominant factors affecting cell performances in IT-PEMFC, of which the drying of MEA is critical, are studied through electrochemical analyses. The optimum ionomer content are suggested regarding on the observation from ionic conductivity and mass transport in chapter 2. Chapter 3 deals with the effect of microstructure change in catalyst layer on the voltage cycling operation of AEMWE. The depth study on mass transport and kinetics of the MEAs for AEMWE are carried out by analyzing the polarization behaviors and electrochemical impedance with varying feed configurations and described in chapter 4. The summary and outlooks of the research works are discussed in chapter 5.

Chapter 2. Investigation of MEAs for IT-PEMFCs Operated at 120 ºC under Low Humidified Conditions (≤ 35% RH)

2.1. Background

In PEMFC operation at intermediate-temperature with low relative humidified gas, MEA drying is dominant and results in poor ionic conductivity and cell performance degradation. Therefore, it is important to maintain hydration by retaining the produced water during electrochemical reaction in the cathode. Ionomer not only binds the catalysts but also conducts ions and absorbs water within the catalyst layer. The higher ionomer content is advantageous to proton conductivity, whereas it is disadvantageous to mass transport by covering the reaction site of catalysts. Therefore, the optimization of ionomer content is important to facilitate effective electrochemical reaction in the catalyst layer. There were several researches on the ionomer content optimization of catalyst layer in LT-PEMFCs. For example, Kim et al. reported that the optimum ionomer content of catalyst-coated-membrane-type MEAs was 35 wt.% at low current density (0.4 A cm^{-2}) and low RH (40%), but decreased to 20 wt.% when the concentration overpotential became more dominant on increasing the current density to 1.2 A cm^{-}

^{2} (larger water production) or the RH to 87% (slower water removal) [46]. Similar trend was also reported for LT-PEMFCs prepared by the decal method [43].

The development and optimization of catalyst layers in IT-PEMFCs have received less attention; only a few studies have been reported, including studies on the effect of additives like ammonium carbonate [91] and PEG [92]. The effects of ionomer contents on the performance of IT-PEMFCs were investigated at 35% [93] and 100% RH [94]. In general, higher cell performances have been achieved at higher RH [94, 95], but a large humidifier is required to maintain the RH. Since larger amount of water is required due to the higher saturated vapor pressure at 120 °C, operation at lower RH would be desirable for IT-PEMFC; therefore, MEA optimization is required for such conditions. The high vapor pressure at 120 °C also largely reduces the oxygen partial pressure; therefore, in IT-PEMFC, the cathode feeds are usually pressurized (0.5–2.0 bar) [29, 92, 94, 96, 97] to provide sufficient oxygen supply, while some studies employ atmospheric pressure [91, 93, 95]. Applying back pressure should also be beneficial in decreasing water removal in electrodes.

There has been no report on the effects of the Aquivion™ ionomer content in the catalyst layer on IT-PEMFC performance under low-humidity operating conditions (< 35% RH). Herein, constructing effective catalyst layers of IT-PEMFC for the low-humidity operating conditions are aimed, and ionic conductivity and mass transport of the fuel cell electrodes were examined with various ionomer content in the catalyst layer. The dependence of single cell performance on

Aquivion™ ionomer contents of the catalyst layer under reduced RH conditions. The effects of RHs (10 – 35%) and inlet gas flow rates (75 – 250 mL min^{-1}) on the IT-PEMFC performance were studied by conducting electrochemical analyses at 120 °C, and the optimum ionomer content of IT-PEMFC was suggested in terms of the ohmic resistance and mass transport in the catalyst layers. The obtained results provide valuable insights on the operation of IT-PEMFCs under low-humidity conditions (< 35% RH) and optimization of its catalyst layer to achieve high efficiency of the PEMFCs.

2.2. Experimental

2.2.1. Preparation of Membrane Electrode Assembly

Commercial and homemade MEAs were used to study the effects of gas flow rate and cathode ionomer content, respectively. Catalyst inks were prepared by mixing a carbon-supported platinum catalyst (Pt 45.7 wt.%, Tanaka K. K.), isopropyl alcohol (A.C.S grade, Burdick & Jackson) and Aquivion™ ionomer solution (D83-06A, Solvay Solexis) to serve as electrodes of the homemade MEAs. The cathode ionomer contents were 20, 30, and 40 wt.% of the total solid weight, while the anode ionomer content was fixed at 30 wt.%. The total solid amount was 0.5 wt.% of the catalyst ink solutions for both electrodes. Then, the MEAs were fabricated by spraying the catalyst inks directly onto the 30 um thickness of Aquivion™ membranes (E87-03S, Solvay Solexis) using an automated system (Gunman, Jeewon Hi-tech). Pt loading was fixed at 0.4 mg cm^{-2} for both the electrode catalyst layers with an active electrode area of 10.24 cm^2. Finally, the MEAs were dried at 60 °C for 30 min in a dry oven.

2.2.2 Electrochemical Analyses

Electrochemical measurements were performed to examine the MEA performance using a high-current potentiostat (HCP-803, Bio-Logic). A single cell

was activated under constant current operation at 0.2 A cm^{-2} before measuring its performance. Galvanostatic method was used to control the water production rate, which is directly related to MEA hydration. When the chronoamperometry was conducted, the current density was slowly increased to 0.2 A cm^{-2} over 2 h to avoid any possible electrode degradation due to sudden cell potential changes. Electrochemical impedance spectroscopy (EIS) was performed in the galvanostatic mode in the frequency range from 10 kHz to 10 mHz, and 10% of the direct current was used as alternating current amplitude under each experimental condition. For single cell analysis, an MEA was assembled with gas diffusion layer (Sigracet 34 BC, SGL Carbon Inc.), Teflon® gaskets, graphite blocks with serpentine flow field, and hard anodizing aluminum end plate. The cell was clamped by eight M8 screw joints with a torque of 4 Nm. Then, the single cell was installed at a fuel cell test station (CNL Energy). The cells were operated in a 1.2-bar back-pressurized system at 120 °C with H_2 and air feeding into the anode and cathode inlets, respectively. For observing the effect of the gas flow rate, cathode flow rate was varied from 70 to 245 mL min^{-1}, while the anode flow rate was fixed at 43 mL min^{-1}. For each gas flow rate, the cell was operated at 35% RH. To analyze the effect of cathode ionomer content on cell performance, the gas flow rates were fixed at 43 and 136 mL min^{-1} for the anode and the cathode, respectively, and the RH was varied from 10 to 35% for both electrodes.

2.3. Results and Discussions

2.3.1 Effect of Gas Flow Rate

The effect of the cathode flow rate on cell performance was investigated using a commercial MEA at the elevated operating temperature of 120 °C. The single cells exhibited an open circuit voltage of ~0.95 V, indicating no significant gas leakage through the membrane, and gradual decrease in cell voltage was observed with increasing current density under various air flow rates (Fig. 2.1.a). The polarization curves display different mass-transfer-limiting currents under various air flow rates. For example, a rapid cell voltage drop was observed at current densities > 0.25 A cm^{-2} at the air flow rate of 70 mL min^{-1}, corresponding to 61% of the theoretical oxygen utilization (35% RH, Fig. 2.1.a). The limiting behavior appeared at current density higher than 0.45 A cm^{-2} for an increased gas flow rate of 105 mL min^{-1}, or 66% of the gas utilization. However, the mass limitation phenomenon was not observed with less than 60% fuel utilization, or with oxygen flow rates higher than 140 mL min^{-1} for the current densities up to 0.48 A cm^{-2}. The rapid cell voltage drop indicates significant concentration overpotential at the cathode generated by insufficient oxygen supply to the electrode due to the insufficient gas flow rates.

The higher flow rates should have one positive effect and one negative effect on cell performances, enhanced O_2 mass transportation [98, 99] and MEA drying [99], respectively. When the current density is low (0.05 and 0.10 A cm^{-2}), the single cell performance deteriorates with increasing gas flow rates because the proton transport is more hindered for decreased hydration in the catalyst layer. For higher current densities, the cell voltages initially increased with increasing flow rate, but it decreased for flow rates above 140 mL min^{-1}. This result indicates that MEA drying is a dominant factor in IT-PEMFCs due to the faster water removal at the high operating temperature of 120 °C. Notably, under high current density (larger water production) and low flow rate (slower water removal), the drying effect became less significant. At current densities of 0.20, 0.24, and 0.38 A cm^{-2}, the highest performances were achieved for flow rates of 105, 140, and 210 mL min^{-1}, respectively; facile mass transport and sufficient ionic conductivity were achieved simultaneously (Fig. 2.1.b).

The ohmic resistance of MEA was further studied using EIS under different cathode gas flow rates. The ohmic resistance of MEA is mainly described in terms of the ionic conductivity related to the MEA hydration levels. The ohmic resistance of MEAs is slightly changed, i.e. by 6%, on increasing the gas flow rate from 70 to 245 mL min^{-1} at 35% RH. The ohmic resistance measured at 0.2 A cm^{-2} implies that ~2% of total cell voltage reduction, i.e. 1.1 mV, was caused by the ohmic overpotential, voltage drop derived from ohmic resistance, when the flow rate of 35% RH gas was increased from 70 to 245 mL min^{-1}. These results imply that proton conduction depends substantially on the cathode flow rate. Similar results were

reported for LT-PEMFC operations. Weng et al. reported that the performance of PEMFCs operated at 50 °C increased with increasing oxygen stoichiometric flow rate [99]. However, when the oxygen stoichiometry exceeded the optimum values, the performance stopped increasing due to increased water removal or dehydration as described above [99]. In addition, large performance drop at high current densities resulted from electro-osmotic drag of water, accelerating membrane dehydration [100].

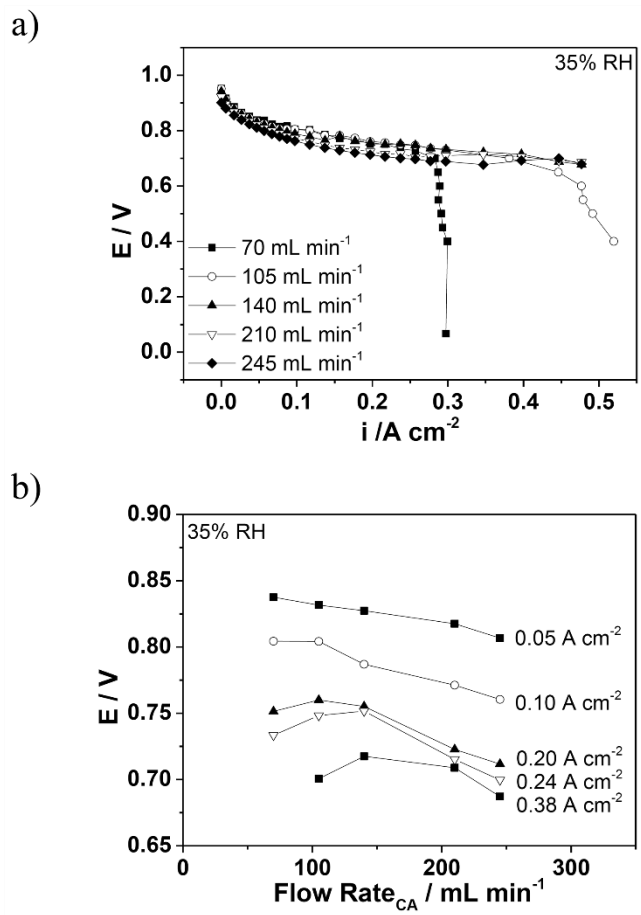

Figure 2.1. a) *i*-V curves with increasing cathode flow rate and b) performances at corresponding current densities under 35% RH.

2.3.2 Effect of Ionomer Content in Cathode Catalyst Layer

As mentioned above, the use of low humidified gas is advantageous for the commercialization of PEMFCs by reducing the size and cost of the humidifier system. Herein the cathode catalyst layer was optimized with different ionomer contents to use the low-RH gas for IT-PEMFCs without suffering significant MEA dehydration and performance degradation. The IT-PEMFC performance was accordingly examined for different catalyst layer ionomer contents at low RH operating conditions. To control the ionomer content of the catalyst layers, MEAs were prepared by the catalyst-coated membrane spray method with 20, 30, and 40 wt. % ionomer contents in the catalyst slurry solution, named AQ20, AQ30 and AQ40, respectively, while the anode ionomer content was fixed to 30 wt.%. However, the catalyst layers prepared with ionomer content higher than 50 wt.% showed cracks on the electrodes, resulting in deteriorated and irreproducible performance.

The cross-sectional and surface images of the as-prepared samples were obtained by scanning electron microscopy (SEM) (Fig. 2.2.). The catalyst layer thickness was approximately 11 μm and did not change significantly for different ionomer contents. However, the electrode surface became smoother with increasing ionomer content in the catalyst layer; similar observations were previously reported by Lei et al. with the Aquivion ionomer™ [101]. Although the structural difference in catalyst layers in terms of different ionomer contents was not recognizable through the magnified images (Fig. 2.2.b and d), the porosity of

the catalyst layer would be lower for higher ionomer contents because the thickness was independent of ionomer content. A previous study on catalyst layers showed that the porosity of catalyst layers decreased with increasing ionomer content [50]. For example, Lei et al. reported the decrease in porosity from 47 % to 8 % with increasing ionomer content from 10 to 40 wt.% without catalyst layer thickness changed [40].

Fig. 2.3. shows the single cell performances recorded in continuous operations with different cathode ionomer contents of 20, 30, and 40 wt.%. Under 35% RH, chronopotentiometry was performed at 0.2 mA cm^{-2} followed by polarization curve measurement. Then, chronopotentiometry and polarization analysis were repeated under RHs of 20% and 10%, as indicated in Fig. 3. The measurements conducted under various RH conditions exhibit that AQ30 showed cell performance loss of ~3% by decreasing RH of inlet gases from 35% to 20% in a constant current operation at 0.2 A cm^{-2}. The performance reduction of AQ20 was more obvious than that of AQ30, i.e. ~5% at the current density of 0.20 A cm^{-2} by decreasing RH from 35% to 20%, implying that higher ionomer contents were essential to achieve high IT-PEMFC performance for low humidification levels. Further, the performance deteriorated more significantly, i.e. > 45%, in all studied samples by decreasing the RH from 20% to 10% because of significant electrode dehydration.

The polarization curves measured after the continuous operations at different RHs are summarized in Fig 2.4. At all RH values of the cathode gases,

AQ40 shows slightly higher performance than AQ20 and AQ30 in regions of low current density (< 0.2 A cm^{-2}). However, the performance of AQ40 decreases faster than those of AQ20 and AQ30 with increasing current density. This polarization behavior implies that dry of the MEA is dominantly affecting the cell performance and only at high current density the relative performance amongst the MEAs with various ionomer content is affected by mass transport limitation from flooding. In other words, the extended ability to absorb more water owing to the high ionomer content of the catalyst layer resulted in poor mass transport at higher current densities; however, this characteristic is beneficial as it moderates MEA dehydration under dry environment, i.e. at low current densities and for low-RH inlet gas flow. The detailed discussion on mass transport limitation by flooding is presented in next paragraph.

Fig. 2.5.a compares the performances of AQ20, AQ30, and AQ40 at low current density, i.e. 0.02 A cm^{-2}, when only a small amount of water is generated and high proton conductivity under dried conditions is important. As discussed above, AQ40 having the highest ionomer content in the cathode catalyst layer showed the best performance at low current densities (0.02 A cm^{-2}), given the proton-conducting ionomer provides a hydrophilic environment and enhanced ionic conductivity in the catalyst layer. However, AQ30 presented the best performance under 35% RH only at high current densities (0.28 A cm^{-2}), in which a large quantity of water was produced and accumulated within the electrodes (Fig. 2.5.b), resulting in mass transport limitation. A similar result was reported by Kim et al.; the performance of cells employing MEAs with high ionomer contents gradually

decreased with increasing level of humidity, implying that the concentration overpotential became the dominant factor in determining the overall humidity dependence of cell performance [46]. However, oxygen transport in the catalyst layer can also be limited in significantly dehydrated environments with low water production rate and low inlet gas RH. For example, Xie et al. reported that low hydration level of the electrode at very low RH reduces oxygen permeability through ionomer agglomerates in the electrode [102]. Therefore, proper hydration level, including the optimum ionomer content, is important for both ionic conductivity and mass transport in the catalyst layer.

In Fig. 2.6, the ohmic resistances of the MEA were determined by EIS. With increasing RHs and current densities the resistance initially decreases because the ionic conductivity is enhanced due to sufficient MEA water contents. However, the ohmic resistances begin to increase at current densities higher than 0.18 A cm^{-2} (10% RH) because water loss due to electro-osmotic drag became more significant compared to back diffusion of water to the membrane. Cheah et al. showed the water activity profile of the membrane at various current densities by modeling the transport of water and protons under electro-osmotic drag [103]. The study showed that the water is removed from the anode by electro-osmotic drag at increased current densities, resulting in membrane dehydration. Moreover, membrane dehydration due to electro-osmotic drag become more serious with insufficient humidification because the amount of back-diffused water is not enough to keep the membrane hydrated [100]. No definite trend of ohmic resistance was found

related to the variation in ionomer content (Fig. 2.6).

Fig. 2.7 shows that AQ40 with the highest ionomer content in the cathode catalyst layer has the greatest apparent *i*R free performance, without considering the ion transfer resistance in the electrolyte membrane. Under the dryer operating condition, where the water production was low at a current density of 0.02 A cm^{-2}, the advantage of loading higher amount of ionomer in the catalyst layer was more clearly revealed. AQ40 and AQ30 exhibited 15 and 77 mV decrease in *i*R free potential, respectively, as the RH decreased from 35 to 10%, whereas the performance of AQ20 was not attested under 10% RH due to significant performance degradations. However, isolating the ionomeric charge transfer resistance of the catalyst layer would be difficult in this system under significantly dried conditions. Liu et al. performed a LT-PEMFC study on proton conduction resistance in the cathode catalyst layer by varying ionomer contents and analyzed the proton resistivity using EIS [43]. In the study, the ionomeric resistance was appeared as 45^{o} segment in the high frequency region of Nyquist plots which is well explained by a transmission line model (TLM) of EIS. The TLM considers both electronic and ionic conduction in the porous catalyst layer employing several identical model elements connected in series, where each segment has an ionic and electronic resistance and capacitance. However, the TLM was not applicable and the 45^{o} segment at high frequencies of EIS plots was not observed in this study under the severe cell operating conditions (120 ^{o}C, < 35% RH). Under the significantly dried conditions, only the catalyst clusters in the vicinity of the membrane-electrode interface would be utilized with considerable *i*R drop in outer

boundary of the catalyst layer. In order to explain the EIS results obtained above, more complex impedance models should be considered with the non-uniform distribution of catalytic activities and ionic conductivities of the porous electrode. Including the numerical modeling of EIS to simulate the porous electrode of IT-PEMFC under dehydrated conditions, research on developing the impedance model would be neccessary to precisely identify different components of the overpotentials with accurate determination of the triple-phase boundary area of the IT-PEMFC electrodes.

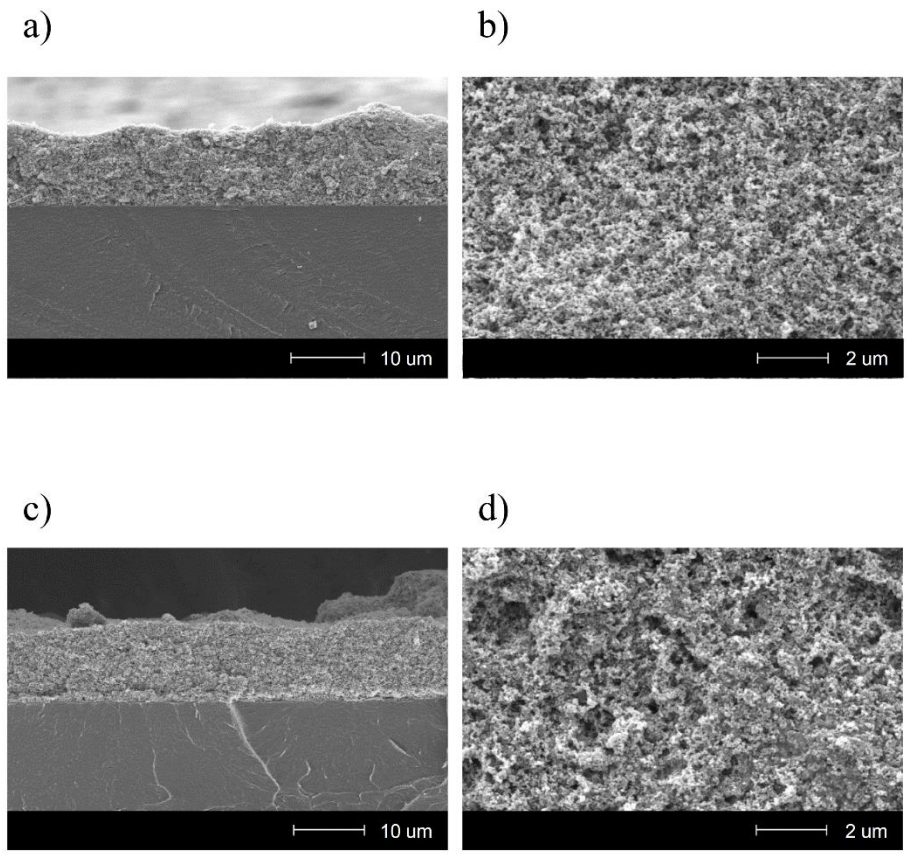

Fig. 2.2. Cross-sectional SEM image of AQ20 (a) and AQ40 (c) and magnified images of the catalyst layer of AQ20 (b) and AQ40 (d).

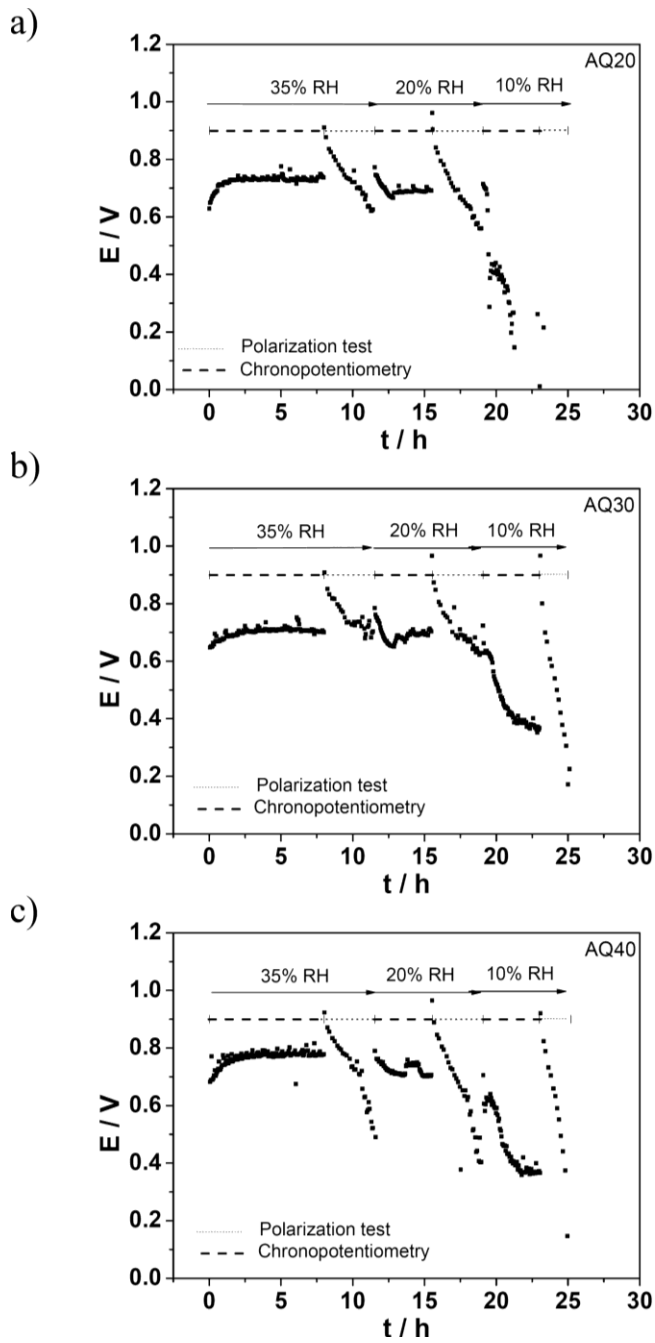

Figure 2.3. A single cell performance during the operation of a) AQ20, b) AQ30, and c) AQ40.

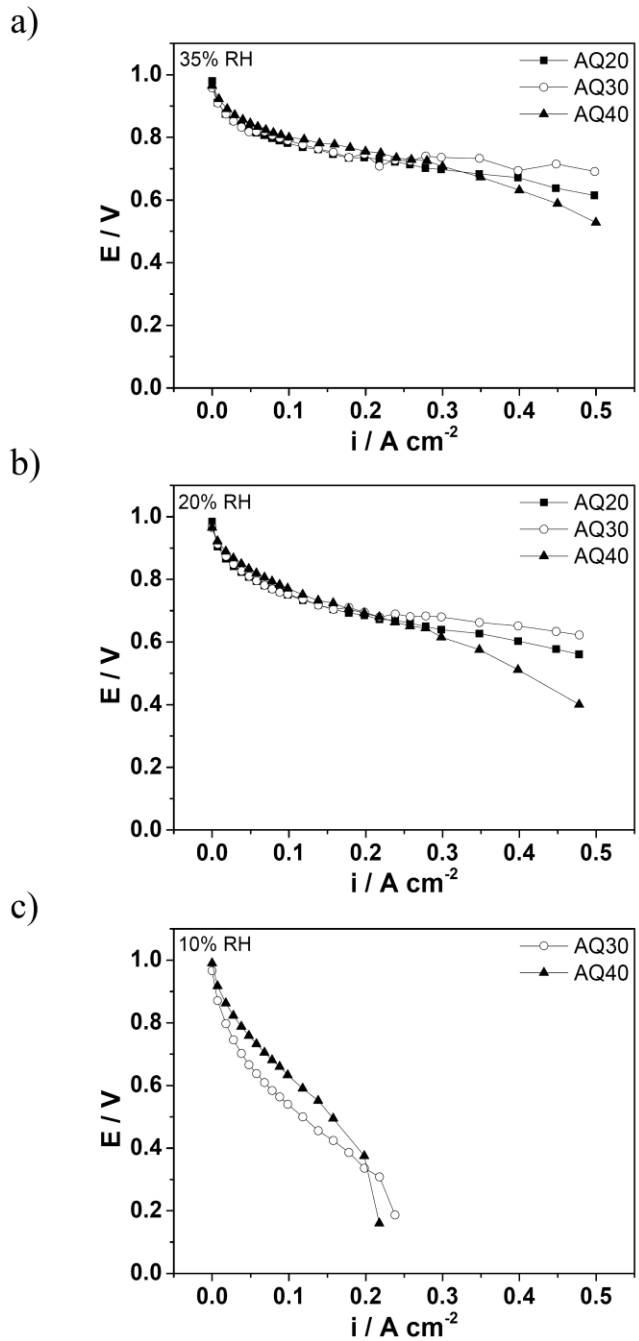

Figure 2.4. *i*-V curves with different ionomer contents at a) 35% RH, b) 20% RH and c) 10% RH.

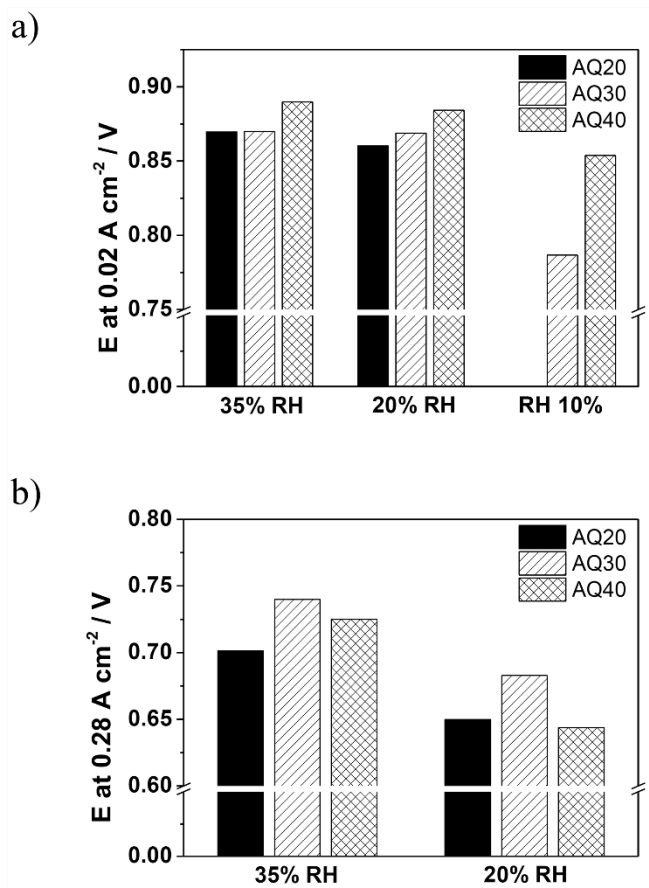

Figure 2.5. Cell voltage comparison of AQ20, AQ30, and AQ40 as a function of relative humidity at different operation current densities of a) 0.02 A cm^{-2} and b) 0.28 A cm^{-2}.

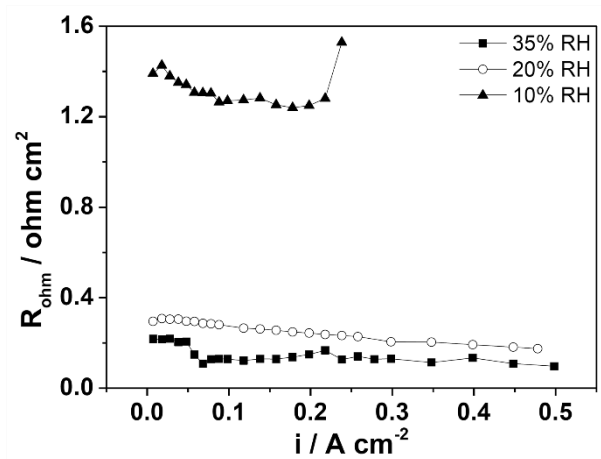

Figure 2.6. Ohmic resistance of AQ30 plot at low relative humidity (10–35% RH).

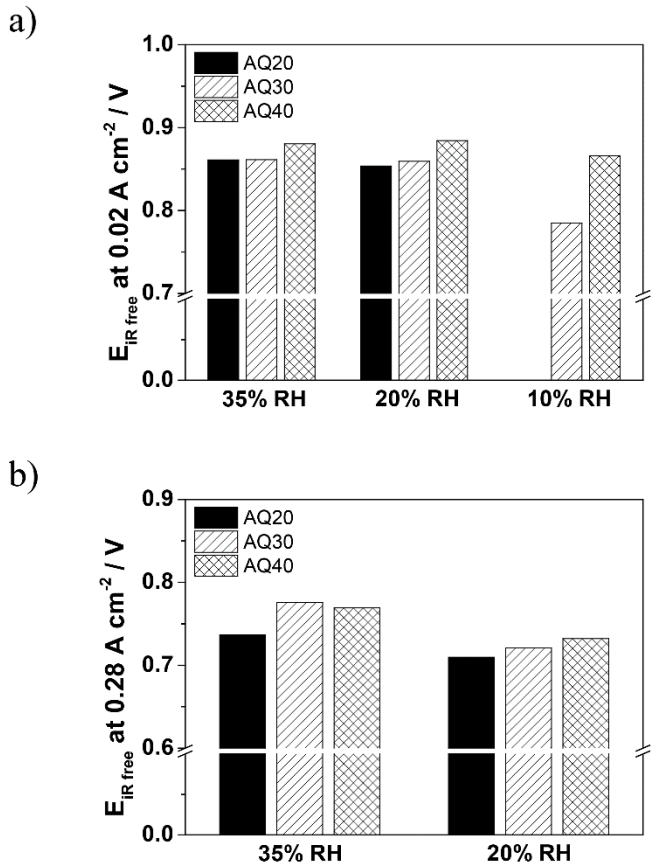

Figure 2.7. *i*R free cell potentials of AQ20, AQ30, and AQ40 with different ionomer contents at cell current densities of a) 0.02 A cm^{-2} and b) 0.28 A cm^{-2}.

2.4. Conclusion

The effects of ionomer contents on IT-PEMFC performance were investigated by conducting single-cell tests and electrochemical analyses at 120 °C under low-RH conditions (10 – 35% RH). In general, cell performance increases with increasing cathode ionomer content due to enhanced proton conduction within the catalyst layer before cathode flooding occurs. The role of ionomer in providing hydrophilic environment in the catalyst layer is further activated in high-temperature operations under low humidified conditions (< 35% RH). The results show that the optimized ionomer content in the catalyst layer is dependent on the operating current density. The optimized ionomer content at the current density lower than 0.2 A cm^{-2} was determined to be 40 wt.% while at the current density higher than 0.2 A cm^{-2} was determined to be 30 wt.%. The presence of higher ionomer contents in the catalyst layer, e.g. 40 wt.%, helps the IT-PEMFCs achieve higher performance, especially under dehydrated conditions. The performance of MEAs becomes more dependent on ionomer content of the cathode catalyst layer under the dehydrated operating conditions, such as the low-RH inlet gas supply and low water production. In other words, optimum ionomer amount in the catalyst layer is the major performance factor in dried cell operating conditions of IT-PEMFCs. In addition, the cathode gas flow rates significantly affect cell performance and membrane dehydration under low-RH conditions, because water removal from catalyst layer and membrane becomes substantial under faster

cathode gas flow. It further implies that the retaining sufficient ionomer contents of the catalyst layer are crucial to secure hydration for high IT-PEMFC performance.

Chapter 3. Investigation of MEAs for AEMWE Operated with Double-side Feed Supplying Method

3.1. Background

In AEMWE operation, fabricating MEAs with high ionic conductivity, low charge and mass transfer resistance for effective electrochemical reaction is one of the key issues to improve the current density. While many previous studies have adopted ionomeric binders in in the MEA electrode of AEMWE single cells, the durability was poor [55, 64, 65, 79, 80]. Polytetrafluoroethylene (PTFE) can be used as a binder for higher durability, as its repeat unit of $–[CF_2–CF_2]–$ has high chemical bond strength and therefore excellent chemical stability [104]. For example, Pavel et al. reported that the AEMWE single cell with PTFE binder [87] delivered initial performance comparable to that with commercial anion-conducting binder (AS-4 ionomer, Tokuyama Corporation) [55], as well as high durability (voltage increase as small as 5% after 500 h). In comparison, the reported voltage increases with ionomeric binders were much higher: 53% for 27 h (AS-4) [55], 24% for 500 h (A-Radel) [55], and 9% for 500 h (polymethacrylate quaternary ammonium ($QPDTB\text{-}OH^-$)) [80]. For the MEAs in polymer electrolyte membrane fuel cells (PEMFCs), the hot-pressing step has been frequently adapted

when fabricating catalyst-coated substrate (CCS) using PTFE-based catalyst layers [105-110], The enhanced cell performances and durability were reported to originate from the reduced resistance at the electrode/electrolyte interface and the suppressed MEA delamination, respectively [109, 110]. However, the study with PTFE-based electrodes in AEMWE by Pavel et al. did not use the pressing step [87]. No study has been reported on the effect of the pressing process in AEMWE systems. However, it is known that when the temperature or pressure is too high, the polymer membrane can be degraded, resulting in decreased conductivity [111]; or the electrodes can become significantly deformed with porosity loss [112].

Meanwhile, controlling the amount of binder in the electrodes has been used to modify the microstructure and increase the performance of various polymer membrane-based electrochemical cells, including PEMFCs [113-116], PBI-based high-temperature PEMFCs (HT-PEMFCs) [86, 117, 118], and alkaline direct ethanol fuel cells (ADEFCs) [119]. Especially, the pore structure changes with the amount of PTFE loading. For example, severe agglomeration of catalyst particles was observed with high PTFE loading [86, 117, 119]. Increased ohmic resistance with higher binder content was also commonly observed. However, the optimal content seems to depend on the electrochemical reactions in each application. In HT-PEMFCs, Jeong et al. obtained the best performance in the MEA containing 20 wt.% PTFE binder, which produced the lowest charge transfer resistance and highest secondary pore volume [117]. In contrast, Li et al. reported that the ADEFC performances were the highest with 5 wt.% PTFE binder in the catalyst layer [119].

Regarding the durability, higher PTFE loading was reported to help prevent the catalyst particle loss in the out-stream during long-term operations [119]. However, the effect of binder content in AEMWE systems has not been reported, since the reported single cell performances were all based on fixed amounts of binders (PTFE: 9 wt.% [87], A-Radel ionomer: 22 wt.%, [55], quaternary ammonium groups modified polymer: 20 wt.% [64], and polysulfone quaternary benzyl trimethylammonium: 30 wt.%).

In this study, the effects of MEA hot-pressing and the binder content (5–20 wt.%) in the anode electrode on the cell performance of AEMWE were investigated, by electrochemical analyses with voltage cycling operation. The characteristics of MEA performance with various catalyst layer structures were observed through polarization curves and impedance. These factors were then optimized to achieve high performance for AEMWE operation, based on the measured electrochemical data.

3.2. Experimental

3.2.1. MEA Preparation

Electrodes in the MEAs were fabricated via the CCS method as follows. The catalyst ink slurry was prepared with the electrocatalysts of IrO_2 (Premion®, Alfa Aesar) and Pt/C (Pt 46.5 wt.%, Tanaka K. K.) for the anode and cathode, respectively. Each electrocatalyst was mixed with isopropyl alcohol (A.C.S grade, Burdick & Jackson), an aqueous solution of PTFE (60 wt.% PTFE dispersion in H_2O, Aldrich), and distilled water. The amount of PTFE in the anode was varied as 5, 9, 12, and 20 wt.% of the total solid weight, while the cathode binder content was fixed at 9 wt.%. The prepared anode and cathode inks were homogenized in an ultrasonic bath for 1 h, and then sprayed onto titanium paper (250 μm in thickness) and carbon paper (TGP-H-120, Toray), respectively. The electrodes were dried at room temperature overnight and then sintered at 350 °C in N_2 gas. During sintering, the molten PTFE improves the binding of catalysts within the electrode. Next, the MEAs were fabricated by sandwiching the anion exchange membrane (A201, Tokuyama) between the anode and cathode electrode.

To study the effect of pressing on the performance of AEMWE, the MEAs containing 9 wt.% PTFE binder were fabricated under three conditions: i) without pressing, ii) pressing at room temperature for 1 min and iii) pressing at 50 °C for 1 min. The hot-pressing temperature of 50 °C was chosen based on the

cell test protocol provided by the supplier of the AEM (Tokuyama Corporation). The applied pressure was 669 psi.

3.2.2 Electrochemical analyses

In the single cell assembly, a titanium plate and a graphite plate were used to supply the electrolyte solution at the anode and cathode sides, respectively. The cell was operated at 50 °C, with 0.5 M KOH and H_2O as the anode and cathode feed solutions at the flow rates of 1 and 3 mL min^{-1}, respectively. The reactant solutions were allowed to flow initially for 10 min before the cell operation in order to hydrate the MEA. Then, the cell potential was controlled using a high-current potentiostat (HCP-803, Bio-Logic). In order to evaluate the cell performance for AEMWE, the cell voltage was cycled in the range of 1.5–2.2 V at a scan rate of 20 mV s^{-1}. Electrochemical impedance spectroscopy (EIS) was used to identify different electrode resistances that affect the cell performance. EIS was conducted at the cell voltage of 1.8 V with an AC frequency range from 15 kHz to 1 Hz and alternating voltage amplitude of 10 mV.

3.3. Results and Discussions

3.3.1. Effect of Pressing Conditions

Three pressing conditions were tested: without the pressing step (P0), pressing at room temperature (P1), and pressing at 50 ℃ (P2). Since the temperature of 50 °C was chosen according to the cell test protocol provided by the membrane supplier, no membrane degradation was expected during the hot-press process. AEMWE experiments carried out by other researchers also demonstrated operation at 50 ℃ or higher temperatures without noticeable degradation, such as those by Leng et al. (50 °C) [55], Ahn et al. (50 – 70 °C) [89, 120], and Pavel et al. (55 °C) [87].

The pressing of the diffusion layer creates a more closely packed structure in the membrane electrodes with reduced pore size, thereby affecting the physicochemical properties of the catalyst layers for water electrolysis [121]. Scanning electron microscopy (SEM, data not shown here) showed that pressing the MEAs (P1 and P2) reduced the thickness of the cathode diffusion layer (carbon paper) by 25% (278 ± 12 μm) relative to the original value (370 μm), while that of the anode diffusion layer (titanium paper) stayed the same (285 ± 17 um). Also, no severe destruction of carbon fibers or visible changes in pore distribution were not observed. The porosity reduction can be determined from the thickness reduction which was expected to be 53% (porosity of TGP-H-120 is 78% according to the

product specification). However, we found that the temperature had no effect on the thickness change. In a previous study of PEMFC, a thinner layer was found to enhance the reactant supply and product removal by reducing the path length for mass transport, but the reduced porosity after pressing could hinder the transport of products and reactants [122]. The hot-pressing process is also known to reduce the interfacial resistance between the electrolyte membrane and electrode, resulting in improved performance in PEMFCs [39]. It is also required in the MEA preparation via CCS method [123]. However, unlike the PEMFC systems which are dominated by gas-phase reactants, AEMWEs operation is carried out in the liquid phase, so the hot-pressing of MEA could have different effects on the cell performance.

To quantify the effect of pressing on the performance, polarization curves of the MEAs were collected by controlling the voltage from 1.5 to 2.2 V as shown in Fig. 3.1. The performance improved during the voltage cycling. P2 exhibited higher water splitting current in the first voltage cycle (243 mA cm^{-2} at 1.8 V, compared to 197 and 195 mA cm^{-2} for P0 and P1, respectively). The current differences between P2 and other MEAs (originally 46–48 mA cm^{-2}) became larger with continued cell operation. For example, in the 25^{th} cycle the current density in P2 is 118 and 77 mA cm^{-2} higher than those in P0 and P1, and the differences further increased to 136 and 92 mA cm^{-2} in the 50^{th} cycle (Figs. 1b and 1c), respectively. The gradual increase of cell performance during operation is underlined by the physical and chemical changes in the membrane and electrodes with the electrolysis. Similarly, the performance enhancement of PEMFCs in continued cell operation has also been reported and attributed to two factors; i)

improved ionic conductivity of the polymer electrolyte membrane as it is hydrated, and ii) increased surface area of the catalyst layer during continued electrochemical reactions [124].

EIS was conducted to elucidate the effects of pressing on the electrochemical performance of AEMWE cells. The Nyquist and Bode plots at 1.8 V in the 50th voltage cycle are given in Fig. 3.2. The ohmic resistance representing the ion transfer resistance was determined from the x-intercept of the high frequency region of Nyquist plot, and the values are similar for P0, P1, and P2 (approximately 0.26 Ω cm^2). The polarization resistances of MEAs, which correspond to the electron transfer resistance during the electrochemical reactions at the electrodes, were determined as the difference between the x-intercepts of high-frequency and low-frequency regions. As shown in Fig. 3.2a, the values are different under different pressing conditions (1.19, 1.11, and 1.04 Ω cm^2 for P0, P1, and P2, respectively), indicating that high-temperature pressing facilitated the electrochemical reactions in the catalyst layers.

An additional semi-circle was observed for P0 in the low frequency range (around 30 Hz) in the Nyquist plot (Fig. 2a). The low-frequency impedance, or the size of the semi-circle, appeared to be smaller in P1 and disappeared in P2, suggesting improved mass transport as previously reported for the hot-pressing process [125] (see discussion below). For example, in the characterization of PEMWE by Dedigama et al. a noticeable second arc was observed at low frequency under high voltage that is associated with mass transport limitation [125]. From the Bode plot (Fig. 3.2b), similar impedance values were obtained for P0, P1,

and P2 at 15 kHz, representing their similar ohmic resistance (average value of 0.341 Ω cm^2). Therefore, the reduced ionic transfer resistance (due to improved interfacial contact between the membrane and electrodes after pressing) was not significant in the AEMWE operation. Additionally, a cusp was observed at 30 Hz on the curve for P0, where the low frequency semi-circle was found in the Nyquist plot, meaning that mass transport resistance exists in the MEAs fabricated without the pressing step. The measured impedance in P1 and P2, in contrast, indicates that the mass transfer resistance has been reduced. In summary, electrochemical observations, including the polarization behavior and measured impedance, imply that the pressing step during the MEA fabrication improves the transport of electrons [126] and mass [127] in the electrode due to the thinner diffusion layer observed through SEM.

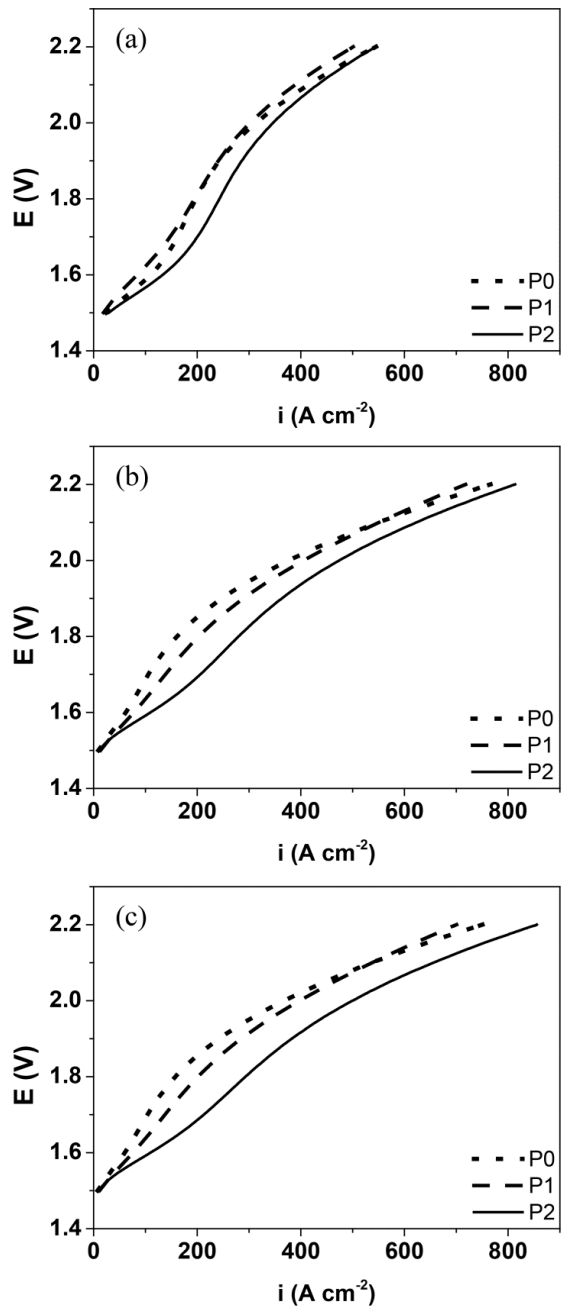

Figure 3.1. *i*-V curves obtained at the (a) 1st, (b) 25th, and (c) 50th cycle for the MEAs fabricated with 9 wt.% PTFE binder in the anode and no pressing (P0), pressing at room temperature (P1), and at 50 °C (P2).

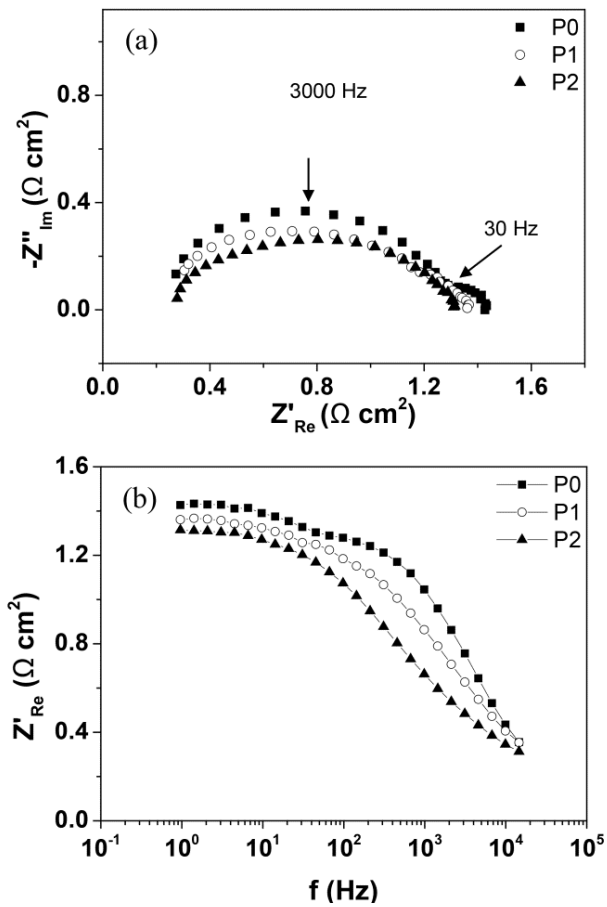

Figure 3.2. (a) Nyquist and (b) Bode plots obtained from EIS measurements at 1.8 V in the 50th cycle (15 kHz–1 Hz) for P0, P1, and P2.

3.3.2. Effect of Anode Binder Content

Next, the effect of PTFE binder content in the anode catalyst layer was examined in order to further optimize the electrode structure for AEMWE. The MEAs were fabricated with varying anode binder contents of 5, 9, 12, and 20 wt.%, named as BC5, BC9, BC12, and BC20, respectively. The pore structure in the electrode of each MEA was investigated by SEM, and displayed in Fig. 3.3. During the annealing at 350 °C in N_2 gas, PTFE melts and is dispersed within the electrodes, thereby binding the nanoparticles to form a catalyst layer. However, at higher PTFE contents more catalyst particles are covered by the binder and become agglomerated. For example, a large number of smaller pores (< 0.13 μm in diameter) were observed with fewer agglomerates (< 0.25 μm in diameter) in BC5, while in BC20 only a low number of larger pores (< 1.02 μm in diameter) were observed with larger agglomerates (< 0.88 μm in diameter). Such secondary pore structure change due to varying binder content was observed by Jeong et al, who found that an increased PTFE content reduces the volume of secondary pores in the catalyst (defined as the space between large agglomerates with the size of 0.08–4 μm, and related to mass transport) while the primary pore distribution (space between small agglomerates with a size of 0.01–0.08 μm) is not affected by the PTFE content [117].

The AEMWE cell performances obtained from voltage cycle measurements are presented in Fig. 3.4. The water splitting current rapidly increased in the first ca. 50 cycles, and the increment was noticeably reduced afterwards for all binder contents. Between the 10^{th} and 50^{th} cycle, the electrolysis current at the cell voltage of 2.2 V was enhanced by approximately 74, 104, 89, and 78 mA cm^{-2} for BC5, BC9, BC12, and BC20, respectively. However, from the 50^{th} to 100^{th} cycle, the respective increments were only 13, 38, 9, and 15 mA cm^{-2}. After ca. the 100^{th} cycle, the cell performance was stabilized.

In the current-voltage behavior of water electrolysis devices, mass transport-limited current is often observed when an insufficient amount of the reactant (i.e., water) is supplied to the reaction sites in the catalyst layer. The gaseous products of water splitting should also be removed efficiently to regenerate the active surfaces in the catalyst layer. The loss of mass transport manifests as exponential growth in the polarization curves, while the activation and ohmic losses are expressed as a logarithmic trend at the beginning and straight sloped line in the middle of the polarization curve, respectively [128]. In the experiments, mass transport limitation was observed in the current density of approximately 200 mA cm^{-2} for BC5, BC9, and BC12 where the S-shape of the polarization curves exhibits the increased overpotentials in their middle. The curves changed to exponential shapes with increasing binder content (Fig. 3.4), indicating that the optimized pore structure facilitated the transport or removal of gas products from the catalyst layer. The removal of mass transport limitations has been explained in terms of gas transport mechanisms in the flow channel of MEAs: efficient gas transport can be achieved

with slug flow in the porous electrode, whereas bubbly flow is considered to induce the mass transport limitations [125]. The mass transport limitation disappeared in the polarization curves, probably by the changed gas transport mechanism when the binder content is increased or after continued voltage cycling operation (Fig. 3.4).

Fig. 3.5 shows the current densities in consecutive voltage cycling operation recorded at 1.6 and 2.2 V for MEAs with different anode binder contents. At 1.6 V, at which the kinetic overpotential dominates the polarization behavior, the performance decreased with cell operation for BC5, BC9, and BC12. However, the reduction in current density from the 5^{th} to 100^{th} cycle became smaller with increased anode binder content (-28, -15, and -5 mA cm^{-2} for BC5, BC9, and BC12, respectively). The current decrease in continued operation can probably be attributed to the loss of catalyst during the reformation of electrode structure in the case of low binder loading. However, performance increase in the process of voltage cycling was observed at 2.2 V, implying favorable structural modification in MEAs during the cyclic operation so to facilitate the mass transport required at high current densities (e.g. at 2.2 V), although the absolute performance of BC20 was significantly lower than other MEAs.

Fig. 3.6 presents the polarization curves at the 100th AEMWE cycle with different anode binder contents. In the *i*R-uncorrected polarization curves at the 100th cycle (Fig. 3.6.a), BC9 showed the best performance, and the difference between it and other MEAs grew with the applied voltage: at 1.6 and 2.2 V, BC9 had a higher electrolysis current density than BC5 by 17 and 223 mA cm^{-2}, respectively. The performance of BC20 was significantly lower than other MEAs, since the excess amount of PTFE in the electrode (20 wt.%) would cover the catalyst surface and hinder the electrochemical reaction.

To study the effect of PTFE binder contents on the electron transfer resistance in the MEAs during AEMWE, the ion transfer resistance was eliminated by using the *i*R-corrected polarization curves (Fig. 3.6.b). In these curves, the performance of BC5, BC9, and BC12 are similar to each other, implying that their performance differences were predominantly caused by the ohmic resistance in the MEAs when the binder content is 12 wt.% or lower. In other words, the charge transfer kinetics of the catalytic reactions are not affected by the binder contents less than 12 wt.% in the catalyst layer. Compared to the performance difference with BC9, the percentage of *i*R drop out of the total potential drop at 100 mA cm^{-2} was 95%, 25% and 1% (i.e., 18 out of 19, 2 out of 8, and 4 out of 383 mV) for BC5, BC12, and BC20, respectively. However, the *i*R-corrected performance of BC20 was significantly lower, suggesting that the active catalytic sites for electron transfer would be blocked by an excess amount of PTFE binder.

Nyquist and Bode plots obtained at 100th cycle for the MEAs with varying anode binder contents are presented in Fig. 3.7. For BC5, BC9, BC12, and BC20, the measured polarization resistances were 1.26, 0.942, 0.945, and 2.64 Ω cm^2, and the ohmic resistances were 0.447, 0.269, 0.274, and 0.637 Ω cm^2, respectively. Both resistances are minimized in BC9, and the trends observed in the resistances versus binder content are in agreement with that for the MEA performance. A high real impedance (0.673 Ω cm^2) at 15 kHz was observed in the Bode plot for BC20 (in Fig. 7b), representing the upward curve shift by the significantly high ohmic resistance. The high resistance is a result of the high loading of non-ionic conducting binder in the catalyst layer. Due to the overpotential caused by the high ohmic and polarization resistances, BC20 showed the lowest performance amongst the MEAs. It has been reported that the PTFE binder in the catalyst layer could support the catalyst, and build the pore structure that is beneficial for the transportation of ions and molecules for the electrochemical reactions [119]. However, an overloading of PTFE binder in the electrode lowered the performance as shown with BC20, since the hydrophobic and insulating PTFE binder impedes the transfer of hydroxide ions and electrons for oxygen evolution reaction, by covering the active surface sites of the catalyst particle [119].

In summary, the electrode structure and mechanism of performance drop under various binder loadings in the anode and pressing parameters were examined. Larger agglomerates with fewer pores are associated with higher binder content (within 5–20 wt.%). The optimal performance was obtained with 9 wt.% binder in the anode. Below 12 wt.% binder content, the MEA performance was dominantly

affected by ohmic overpotential, while at 20 wt.% binder content it mainly depends on activation or concentration overpotential. The hot-pressing process was found to enhance the performance by facilitating mass and charge transfers.

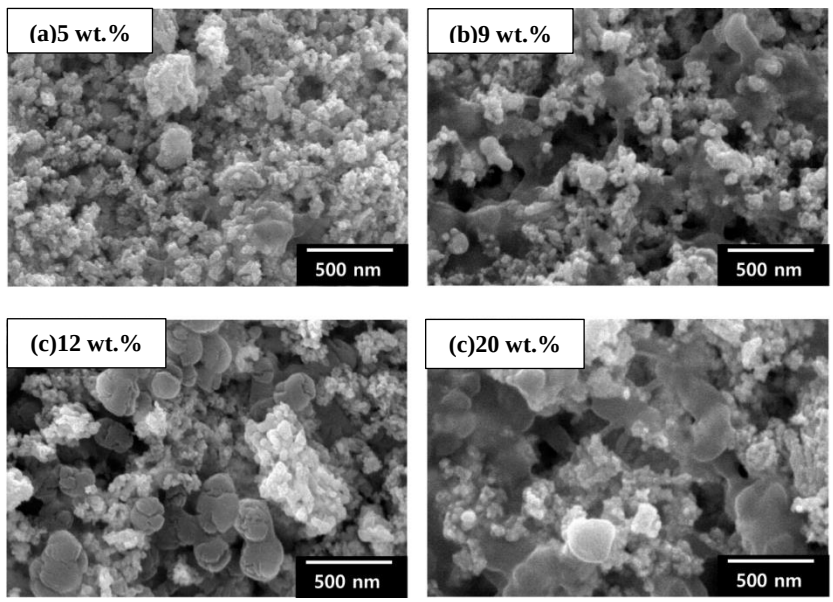

Figure 3.3. Surface SEM images of pristine (a) BC5, (b) BC9, (c) BC12, and (d) BC20 anodes.

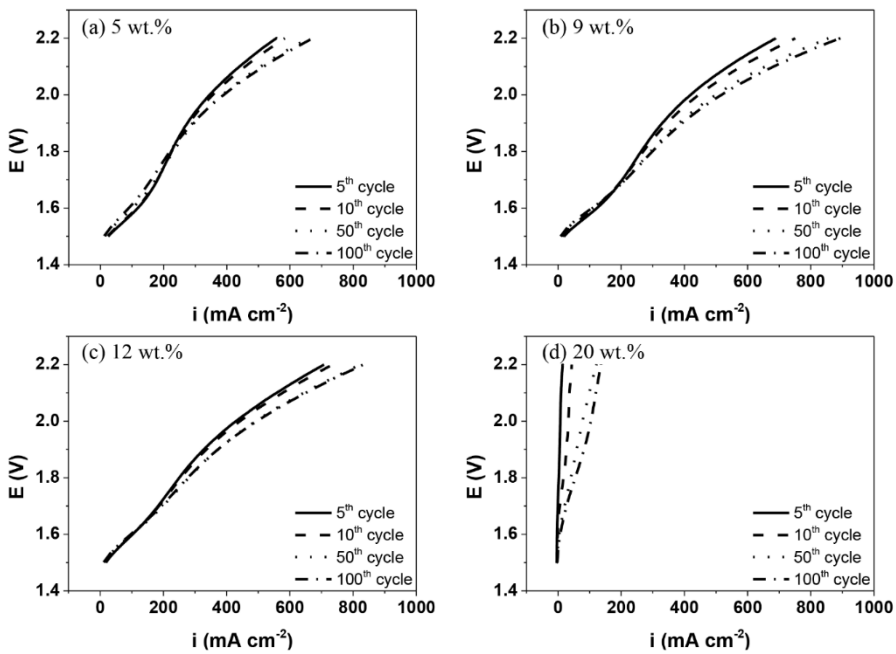

Figure 3.4. i-V curves for voltage cycling operation of MEAs with (a) BC5, (b) BC9, (c) BC12, and (d) BC20, fabricated by pressing at 50 °C.

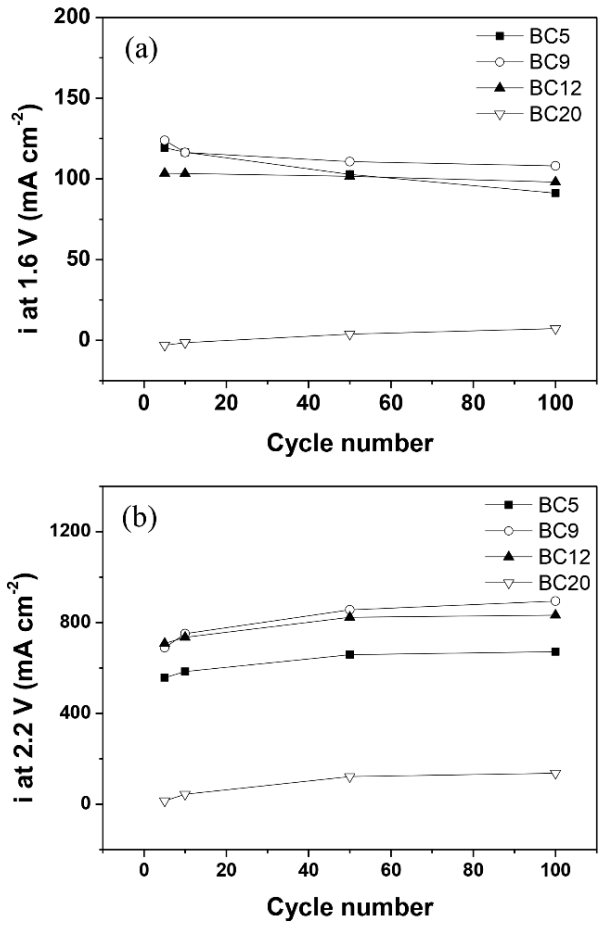

Figure 3.5. Performances at (a) 1.6 V and (b) 2.2 V in voltage cycling operation of the MEAs with different binder contents in the anode and fabricated by pressing at 50 °C.

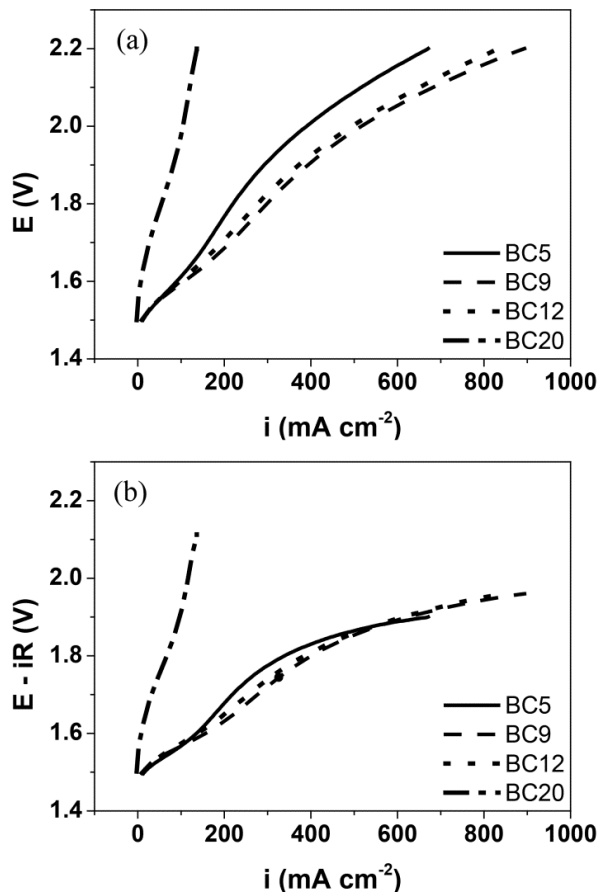

Figure 3.6. Polarization curves at the 100th cycle obtained (a) without and (b) with iR corrections, for the MEAs with different binder contents in the anode and fabricated by pressing at 50 °C.

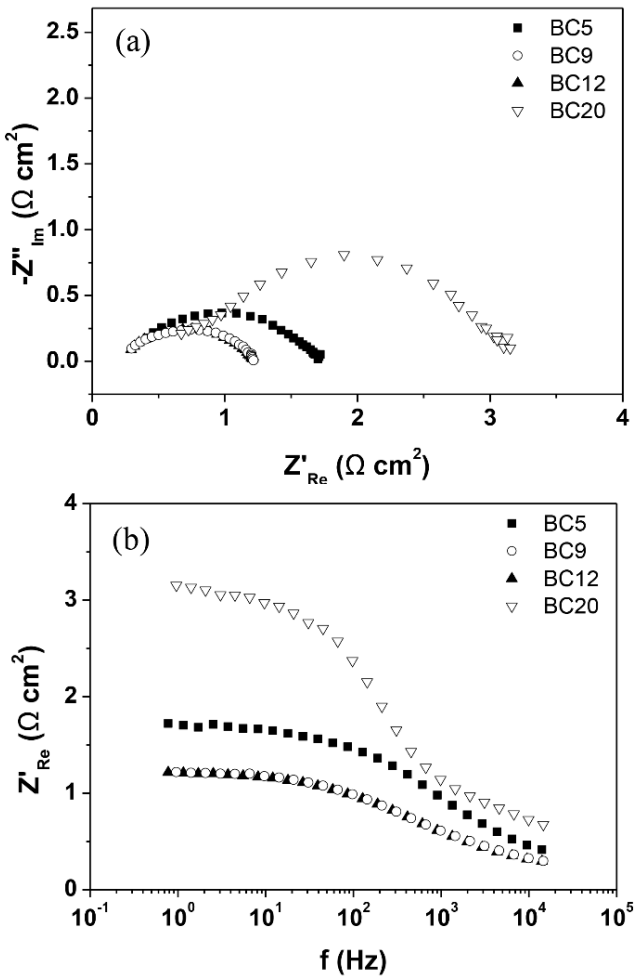

Figure 3.7. (a) Nyquist and (b) Bode plots obtained from EIS measurements taken at 1.8 V in the 100th cycle of the MEAs with different anode binder contents in the anode and fabricated by pressing at 50 °C.

3.4. Conclusions

The effects of pressing conditions and PTFE binder content on the MEA performance for AEMWE were examined for the first time, by operating the cell with potential cycling and electrochemical analyses. Pressing the MEA at 50 °C resulted in a cell performance that is 1.9 times higher than the case without pressing, due to the reduced polarization resistance (by approximately 12%) in the former. The anode binder content in the anode catalyst layer also affects the cell performance, as it changes the ohmic and polarization resistances of the MEAs. The resistances and cell performance are inversely proportional to each other. An insufficient binder loading could not form the secondary pores efficiently, resulting in poor mass transport. On the other hand, overloading the binder impeded the electrochemical reaction by covering the active sites of the electrocatalysts and also hindered the transport of hydroxide ions and electrons. The optimal PTFE binder content was found to be 9 wt.% for the studied range (5–20 wt.%).

Chapter 4. Investigation of MEAs for AEMWEs Operated with Single-side Feed Supplying Method

4.1. Background

Operating the cell at higher temperature improves the reaction kinetics [78, 87, 88], introducing electrolyte solution instead of ultrapure water enhances the OH^- conduction [55, 88], and single sided or double sided feed supplying affects the ohmic resistances [55]. Cell performances of AEMWE are highly dependent on the operating conditions, such as, cell temperature, electrolyte solution and feed type. Operating the cell at higher temperature than the thermally stable temperature of the membrane or binder causes degradation of the materials, introducing high concentrated alkali solution also degrades membrane of MEA in a single cell which resulted in performance degradation. Therefore, operating at appropriate conditions regarding on the properties of materials employed in the AEMWE cell are necessary. The feed type of AEMWE cell operations are varied as double-side feed supply to both anode and cathode [67, 129] or single-side feed supply to either anode [55, 60, 87, 130] or cathode [55, 89, 120] only. Single-side feed to anode uses back diffused reactants from cathode to anode for HER and therefore, the feeding method has an advantage in collecting dry hydrogen gas at cathode, which

eliminates extra process to separate produced hydrogen from liquid. The absence of cathode feed during the operation improves the exhaust of produced gas, which enhances water splitting current by enhancing the mass transport. Leng et al. conducted a study of performance dependency on feed type with the developed ionomer applied MEAs under three different feed configurations, which were introducing pure water to anode only (case 1), cathode only (case 2) or cathode for 2 hours then changing the feed to anode (case 3). They have observed that decrease in ohmic resistance during the cell operation majorly affected the cell performance degradation and best durability was obtained with the case 3 feeding type [55]. No detailed discussion on activation or mass transport overpotentials arisen from the catalyst layer regarding on the feed configuration was not discussed in their study.

In the case of double-side feed supplying method, higher electrode utilization and shorter produced gas exhaust distance are expected by supplying reactants from the surface of cathode diffusion layer. In the case of single-side feed supplying method, lower electrode utilization and longer produced gas exhaust distance are expected but the higher hydroxide ion concentration in the cathode and easier produced gas exhaust are expected from the absence of cathode feed and only the back diffused reactants from anode is participated in the electrochemical reaction. This chapter is focused on the investigation of catalyst layer during AEMWE operation. The effects of feeding configuration and the binder content (5–20 wt.%) in the anode catalyst layer on the cell performance of AEMWE were examined through conducting electrochemical analyses. The performance

influencing factors of operating conditions and MEAs were investigated through analyzing polarization curves and impedance.

4.2. Experimental

4.2.1. MEA Preparation

MEAs were fabricated by pressing membrane (A201, Tokuyama) with catalyst layers prepared through CCS method at 50 °C. The mixture of isopropyl alcohol (A.C.S grade, Burdick & Jackson), an aqueous solution of PTFE (60 wt.% PTFE dispersion in H_2O, Aldrich), distilled water and electrocatalysts were sonicated in an ultrasonic bath for 1 h before sprayed onto substrate. The electrocatalyst of IrO_2 (Premion®, Alfa Aesar) and Pt/C (Pt 46.5 wt.%, Tanaka K. K.) were used for the oxygen evolution reaction (OER) and the hydrogen evolution reaction (HER), respectively. The OER catalyst ink slurry was sprayed onto titanium paper (250 μm in thickness) with the PTFE binder content of 5, 9, 15 and 20 wt.% (ratio to the total solid weight). The HER catalyst ink slurry was sprayed onto carbon paper (TGP-H-120, Toray) with the fixed binder content of 9 wt.%.

The catalyst layer prepared through CCS method were dried at room temperature overnight before sintering them at 350 °C under N_2 gas condition. The sintering process improves bindings of catalysts and PTFE within the electrode by producing molten PTFE. The pressing method was introduced based on the results obtained from the previous electrochemical analyses and the detailed information can be found in Chapter 3.

4.2.2 Electrochemical Analyses

In the single cell assembly, a titanium plate and a graphite plate with parallel and serpentine flow filed were used as current collectors for anode anod cathode, respectively. The cell was operated at 50 °C and three different types of feed configurations for cathode were tested, which were supplying i) H_2O for both initial and operating feed, ii) H_2O for initial feed only and no feed supplying during operation, and iii) 0.5M KOH solution for initial feed only and no feed supplying during operation. Cathode feeds were supplied at the flow rate of 3 mL min^{-1} while 1 mL min^{-1} of 0.5M KOH solution was constantly introduced to anode for all of the three feed types.

To achieve sufficiently hydrated MEAs before the cell operation, initial feeds were supplied for 10 min before starting the experiments. The cell was operated with voltage cycle from 1.5 to 2.2 V at a scan rate of 20 mV s^{-1} to evaluate the cell performance. EIS was employed to determine the ohmic resistances and polarization resistances affecting the cell performances for different operating conditions and catalyst layer fabrication conditions. EIS was conducted at 1.8 V with alternating voltage amplitude of 10 mV in the AC frequency range from 15 kHz to 1 Hz. For the electrochemical analyses, a high-current potentiostat (HCP-803, Bio-Logic) was used to control the cell voltage and measure impedance.

4.3. Results and Discussions

4.3.1. Effect of Feed Configurations

The tests on three feed configurations for cathode were experimentally conducted: supplying H_2O as initial and operating feed (F1), supplying H_2O as initial feed only (F2) (no feed supplying during the cell operation), and supplying 0.5M KOH solution as initial feed only (F3) (no feed supplying during the cell operation). The single side feeding method to anode uses the back diffusion mechanism through the membrane to produce dry hydrogen in the cathode. By applying this feeding method, the improvement in mass transport of produced hydrogen gas is expected with dry of cathode catalyst layer. The anode single side feed supplying method were applied in AEMWE operation by other researchers also and the examples can be found in the studies carried out by Faraj et al. [65], Pavel et al.[87] and Parrondo et al. [130].

AEMWE cell performances regarding on feed configurations were investigated during voltage cycling operation using the MEAs containing 20 wt.% and 9 wt.% of PTFE binder in anode and cathode, respectivley. Cell voltages were plotted in the function of current density as presented in Fig. 4.1. F3 exhibited the best performance (32 mA cm^{-2} at 1.8 V) while F1 and F2 showed low performances (2.54 and 0.65 mA cm^{-2} at 1.8 V, respectively) at 5^{th} cycle (Fig.

4.1.a). The high initial performance of F3 was derived from reactant supply, KOH, as initial feed before the cell operation. Rapid performance improvement in F2 and F3 were observed with increasing cycle number. Compared to F1, F2 showed three and six times higher current density which resulted from eliminating cathode operating feed (46 and 55 mA cm^{-2} at 1.8 V was observed for 50^{th} and 100^{th} cycle of F1 while 156 and 321 mA cm^{-2} at 1.8 V was observed for 50^{th} and 100^{th} cycle of F2). In order to determine performance influencing factors regarding on the feed configuration, EIS at 1.8 V was performed.

EIS was performed to monitor the change in ohmic resistances which is directly related to ionic conductivity, with increasing voltage cycling number. Ohmic resistances were decreased from 1.12 to 0.67 Ω cm^2, 1.42 to 0.31, and 0.42 to 0.14 Ωcm^2 during 100 number of voltage cycling operation for F1, F2 and F3 in Fig. 4.2. The rapid reduction in the ohmic resistances was observed in first 10 voltage cycling indicating the increase in OH^- concentration through electrochemical reactions. The introduction of H_2O during cell operation hinders further reduction of ohmic resistances and improvement of cell performance.

Polarization curves were further analyzed with EIS data to determine activation and concentration overpotential regarding on the feeding conditions. The equation for reversible cell voltage was firstly derived from the Nernst equation (Eq. 1) where E^o is the standard cell potential, R is the universal gas constant (8.314 J K^{-1} mol^{-1}), T is the temperature in kelvins, n is the number of moles of electrons transferred in the electrochemical reaction, F is the Faraday constant

($9.648x10^4$ C mol^{-1}) and K is the equilibrium constant [131]. The cell potentials for alkaline water electrolysis were calculated based on the following derived equation (Eq. 2 and 3) which were determined to be 1.229 V at pH 13.7 (0.5M KOH).

$$E = E^o - \frac{RT}{nF}\ln(K) \quad (1)$$

$$E^o_{Ca} = -0.828 - 0.000198 \text{ x } T \text{ x } (pH\text{-}14) \quad (2)$$

$$E^o_{An} = 0.401 - 0.000198 \text{ x } T \text{ x } (pH\text{-}14) \quad (3)$$

Polarization curves can be expressed as in the Eq.4 where A is the Tafel slope, i_n is the leakage current density, i_0 is the exchange current density and R_{ohm} is the ohmic resistance. The activation over potential (η_{act}) was determined using Bulter-Volmer equation and Tafel plot. The ohmic overpotential (η_{ohm}) was calculated using the ohmic resistance from the high-frequency intercept in the Nyquist plot of impedance data. Concentration overpotential (η_{conc}) was determined as the remaining voltage loss in the polarization curve. The calculated η_{act} and η_{conc} were plotted in Fig. 4.3.

$$E(i) = E^o - \eta_{act}(i) - \eta_{ohm}(i) - \eta_{conc}(i)$$

$$= E^o - A\log(\frac{i + i_n}{i_0}) - iR_{ohm} - \eta_{conc}(i) \quad (4)$$

Activation overpotentials (Fig. 4.3.a) were decreased from 0.438 to 0.413 V, 0.352 to 0.313 V and 0.305 to 0.301 V at 100 mA cm^{-2} from 50^{th} to 100^{th} cycle for F1, F2 and F3, respectively. The largest reduction was observed in F2 indicating the reaction kinetics has been improved mostly compared to F1 and F3. F3 showed the lowest η_{act} since the sufficient OH^- ions were provided by supplying KOH solution as initial feed. F1 showed the highest η_{act} indicating that the reaction rate is slowest and resulted in the lowest cell performance. The dilution of OH^- ions in cathode due to the supply of H_2O during the cell operation is expected. Concentration overpotentials were plotted in Fig. 4.3b. From this plot, the concentration overpotential of F2 and F3 at 100^{th} cycle is minor issue while that of F1 was significantly (0.274 V for F1, 0.035 V for F2 and 0.026 V for F3 at 100 mA cm^{-1}) meaning mass transport is more facilitated in no supplying cathode operating feed condition. Concentration overpotential increases with increasing current density since more of reactant is required under higher current for electrochemical reaction. Single side operating feed to anode showed advantages in not only ohmic resistances, but also electron transport and mass transports. Back diffused reactants from anode to cathode and the produced OH^- through electrochemical reaction in the cathodes resulted in performance improvement.

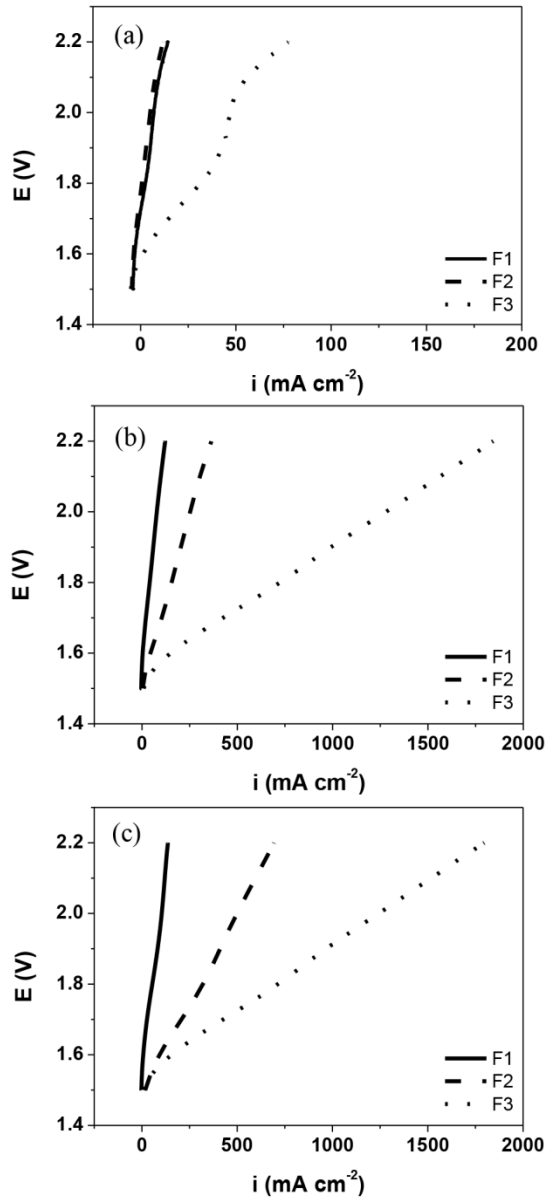

Figure 4.1. *i*-V curves obtained for MEAs fabricated with 20 wt.% and 9 wt.% PTFE binder for anode and cathode, respectively (BC20) at (a) 5st, (b) 50th and (c) 100th cycle for the MEAs operated with supplying H_2O as both initial and operating feed for cathode (F1), supplying H_2O as initial feed only (no operating feed) (F2), and supplying 0.5M KOH solution as initial feed only (F3) at 50 °C.

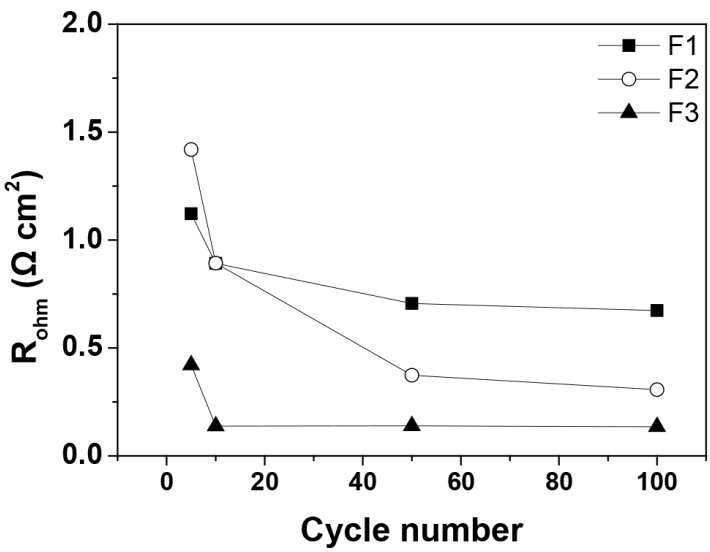

Figure 4.2. Ohmic resistances obtained from EIS measurement at 1.8 V presented in for the MEAs operated under different feeding method of AEMWE operating at 50 °C.

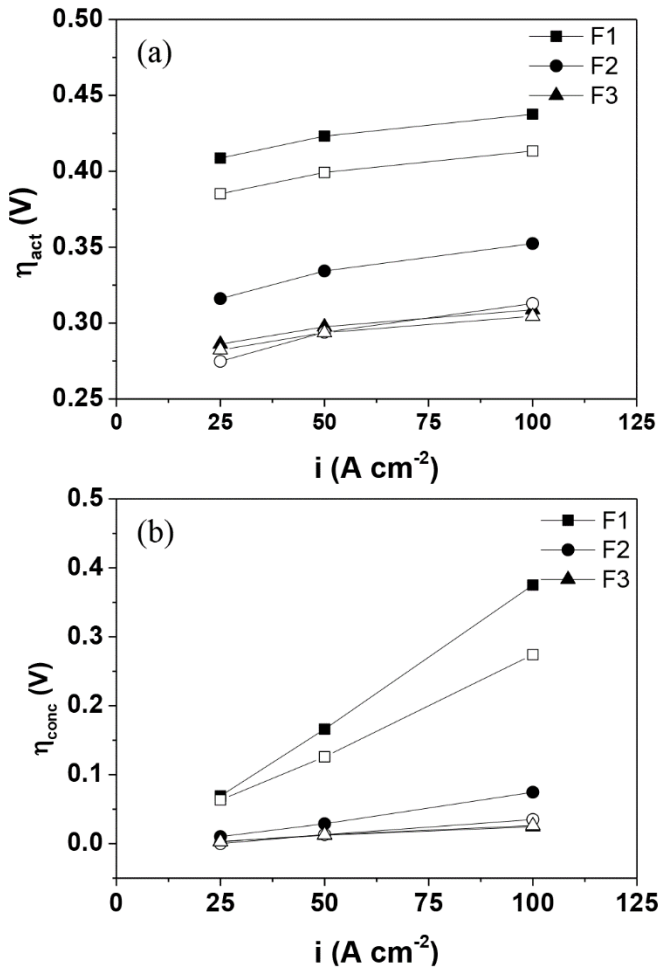

Figure 4.3. Overpotentials calculated from tafel plots for different feeding method: (■ - 50th cycle with F1; □ - 100th cycle with F1; ● - 50th cycle with F2; ○- 100th cycle with F2; ▲- 50th cycle with F3; ∆ - 100th cycle with F3).

4.3.2. Effect of Anode Binder Content

In Chapter 3, the effect of PTFE binder content was investigated with supplying H_2O as operating feed. The current density has been improved by six times by discontinuing the cathode supply feed during the cell operation and using back diffused reactants from anode in the cathode. Higher current density produces higher rate of gas and therefore, poor long-term stability is expected with lower PTFE binder content. Therefore, the effect of PTFE binder content was re-examined in F2 operating conditions. The MEAs were fabricated with the anode binder contents of 5, 9, 15 and 20 wt.%, named as BC5, BC9, BC15 and BC 20, respectively. Before conducting the cell operation, the pore size distributions of catalyst layers were examined through mercury porosimetry instrument. Pore size diameter intensity peak is shifted toward larger pore diameter size with increasing binder content (0.11, 0.14, 0.17 and 0.22 um of pore size diameter are mostly presented for BC5, BC9, BC15 and BC20, respectively) as shown in Fig. 4.4.

The AEMWE cell was operated with voltage cycle in the range of 1.5 – 2.2 V and the current densities obtained at 1.8 V were plotted in Fig. 4.5. BC5 and BC9 showed the high water splitting current densities in the beginning of the cycles (1026 and 989 mA cm^{-2} at 1.8 V for BC5 and BC9, respectively), but water splitting current was rapidly decreased in the first 50 cycles. On the other hand, BC 15 and BC20 showed poor performance in the beginning, but the performance was rapidly improved in the first 150 cycles (573 and 415 mA cm^{-2} of current density

improved for BC15 and BC20, respectively). In the previous chapter, BC9 exhibited the best performance and no performance degradation was observed during 100 voltage cycles. The high current from the initial cycle which value is three times larger than F1 operating condition is achieved with F2 operating condition. However, the performance of BC9 rapidly decreased. The water splitting current of BC 20 kept increased until 1300 cycle and obtained the best performance of 1069 mA cm^{-2} at 1.8 V. The pore structure destruction and catalyst loss was expected from the initial high current density of BC5 and BC9 whereas the increasing current densities with voltage cycle operation restructured the catalyst layer of BC15 and BC20 resulted in performance improvement. Additionally, longer duration was required to achieve the maximum water splitting current with the MEA fabricated with higher binder content.

The current densities at 1.6 V and 2.2 V for different binder contents were plotted in Fig. 4.6. The performance at low voltage is affected by activation losses dominantly while the performance at high voltage is affected by mass transport losses dominantly. At 1.6 V, performances were decreased for BC5 and BC9 with voltage cycling operation while performances were improved for BC 15 and BC20. The highest current density increase of 636 mA cm^{-2} at 1.6 V was obtained with BC20 which indicates kinetic improvements. Similar performance of BC5 and BC9 were presented until 500 cycles, then, that of BC5 decreased faster than BC9. The water splitting current decrease during the operation can probably be influenced by the loss of catalyst during the reformation of electrode. The

destruction of molten PTFE binder is washed off with catalysts by the feed supplied. Therefore, sufficient PTFE binder is required to avoid the loss of catalyst during the cell operation under high current. Similar performance trend was observed at 2.2 V. The current density of BC5 and BC9 were constantly decreased with cell operation while rapid increase in current density of 1003 and 592 mA cm^{-2} during first 200 cycles was observed for BC15 and BC20, respectively. The performance of BC15 was stabilized from 1000^{th} cycle (1515 mA cm^{-2}) while that of BC20 was increased to 1920 mA cm^{-2}. The covered electrochemically active surface area of catalysts are exposed and the pore structures are changed to favorable for mass transport during the reformation of catalyst layer structure. The gradual increase of water splitting current in high binder content containing MEAs improved the cell performance. However, the rapid increase of water splitting current in low binder content containing MEAs resulted in poor long-term stability from loss of catalyst and mass transport limitation.

Performance decay rates were calculated based on the current change between 1400^{th} and 1600^{th} cycle to observe long-term stability of cell performance regarding on the binder content of anode catalyst layer. 0.07 %, 0.04 %, 0.02 % and 0.01 % of performance was decreased for each cycle with BC5, BC9, BC12 and BC20, respectively as presented in Fig. 4.7. Performance decay reduced with increasing binder content. Long-term stability of cell performance is influenced by binder content of anode catalyst layer.

To analyze the catalyst loss with voltage cycle operation, the outlet solution of anode for BC9 and BC20 were collected. The solutions were analyzed using an inductively coupled plasma tandem quadrupole mass spectrometer (ICP-QMS) to trace metal loss (Fig. 4.8). The high catalyst loss of 11 μg_{It} $kg_{solution}^{-1}$ was observed at the 5^{th} and 10^{th} cycle. The loss amount reduced to 1.57 μg_{It} $kg_{solution}^{-1}$ from 20^{th} cycle and constantly decreased with operating the cell for BC9. 0.2 μg_{It} $kg_{solution}^{-1}$of catalyst loss was observed at 5^{th} cycle and from 50^{th} cycle no catalyst loss was observed. This results support the rapid performance degradation in MEAs fabricated with the low binder content.

Ohmic resistances were plotted with different binder content. Ohmic resistance represents the iononic conductivity of MEA which is mainly arisen from the membrane. EIS measurements were performed at 1.8 V and ohmic resistance was collected from the data. BC15 and BC20 showed high ohmic resistance in the initial cycle. Then, rapid decrease in ohmic resistance was observed in first 100 cycles. This large ohmic resistance changes are matched to the rapid performance improvement in the beginning of the voltage cycle for AEMWE of BC15 and BC20. BC5 and BC9 showed low ohmic resistances of 0.18 Ω cm^2at 100^{th} cycle. No sudden change in ohmic resistances of BC5 and BC9 were observed indicating that the performance reduction of BC5 and BC20 was mainly caused from degradation in catalyst layer (Fig. 4.9).

In summary, the performance characteristics on feed configuration change and performance degradation mechanism were investigated under single side anode

feed supplying method. Eliminating cathode operating feed supply enhances ionomer conductivity, reaction kinetics and mass transport. Under this operating condition, higher durability was observed with MEAs fabricated with higher binder content in the anode. Insufficient binder content (below 9 wt.%) resulted in rapid performance degradation by catalyst loss and pore structure destruction.

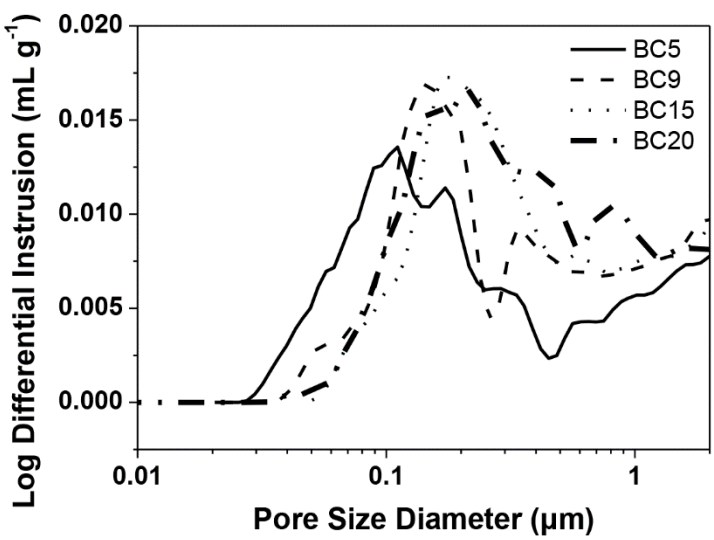

Figure 4.4. Pore size distribution analyzed through mercury porosimetry for MEAs fabricated with 5 wt.% (BC5), 9 wt.% (BC9), 15 wt.% (BC15) and 20 wt.% (BC20) PTFE binder.

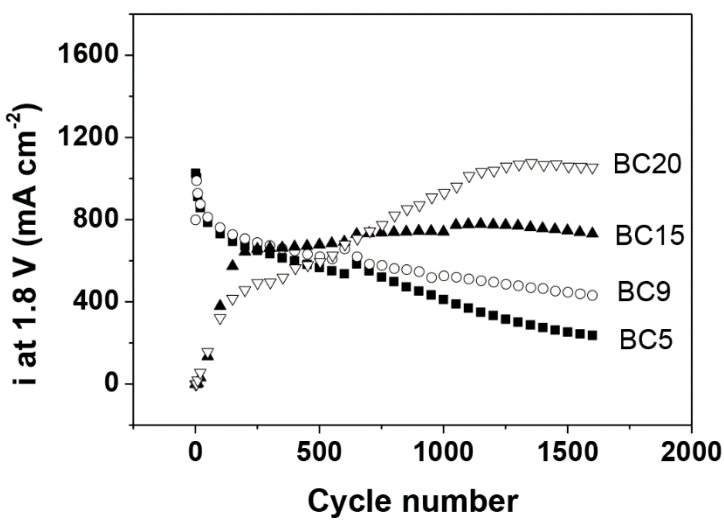

Figure 4.5. Current densities at 1.8 V collected during voltage cycling operation of MEAs fabricated with 5 wt.% (BC5), 9 wt.% (BC9), 15 wt.% (BC15) and 20 wt.% (BC20) PTFE binder in the anode, supplying initial feed of H_2O only to cathode (F2).

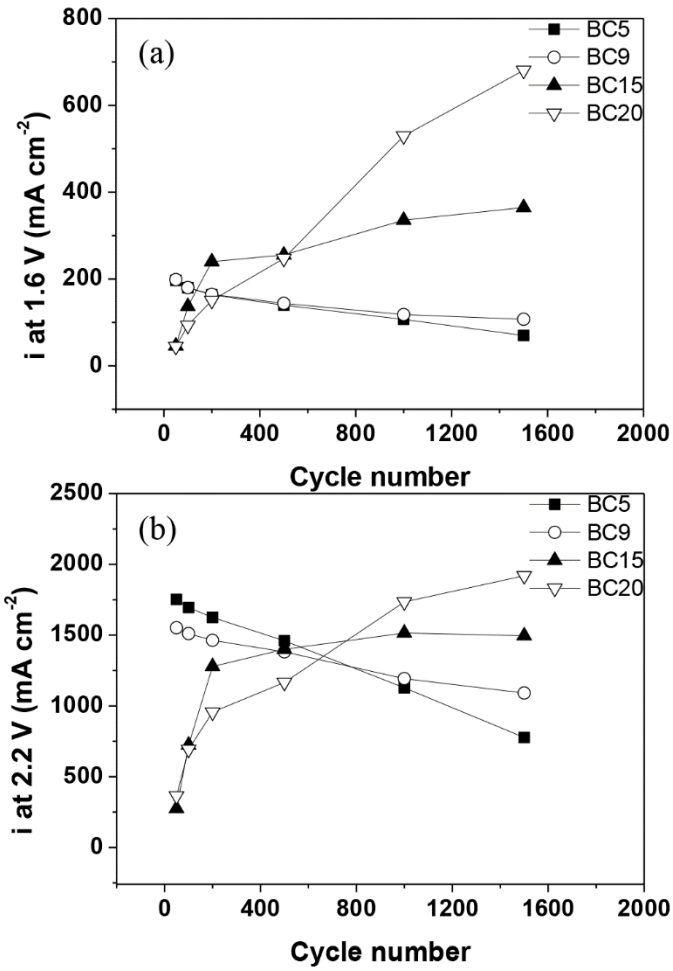

Figure 4.6. Current densities at (a) 1.6 V and (b) 2.2 V voltage cycling operation of the MEAs with different binder contents in the anode.

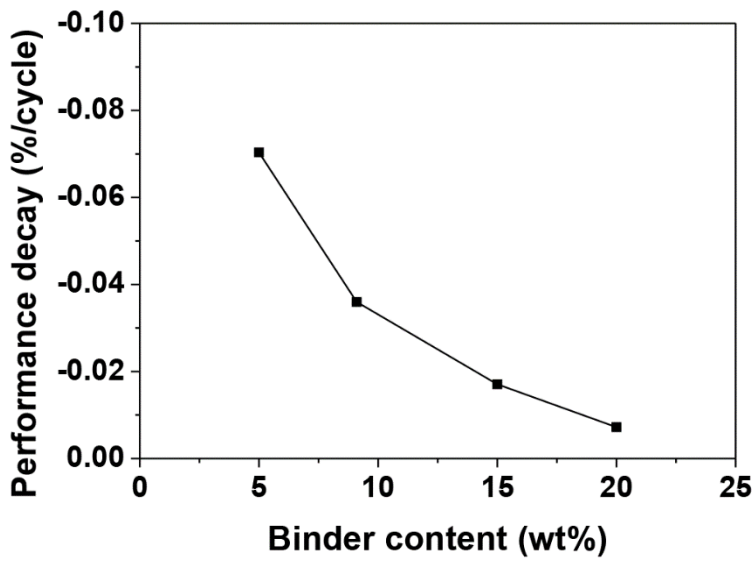

Figure 4.7. Performance decay calculated from 1400th to 1600th cycle with various binder contents.

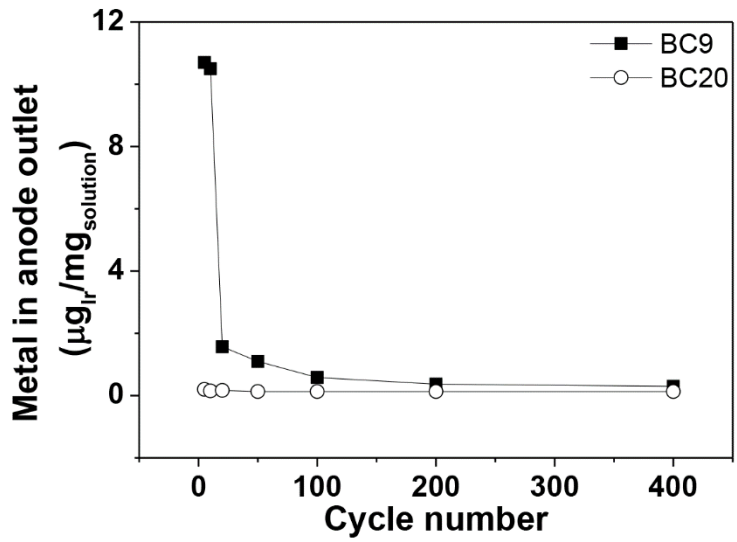

Figure 4.8. Metal presented in anode outlet solution in continuing cell operation.

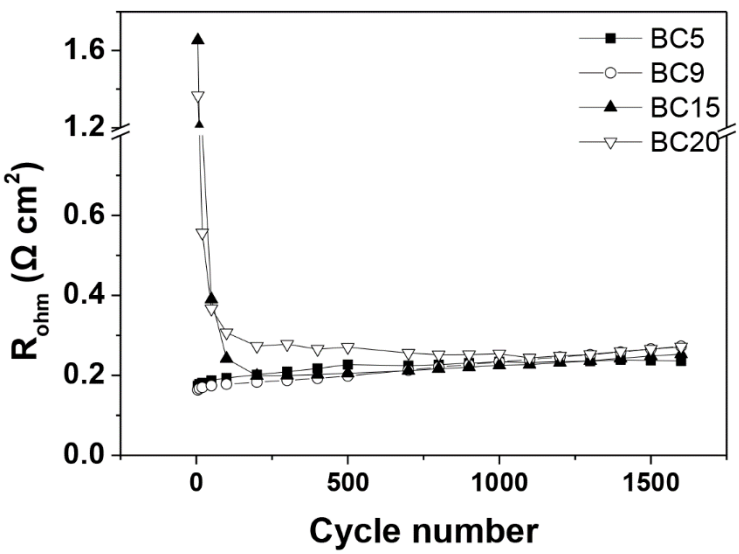

Figure 4.9. Ohmic resistances obtained from EIS measurement at 1.8 V with voltage cycling operation for different binder content in the anode.

4.4. Conclusions

The studies of feed configuration and PTFE binder content on the single cell performance for single side anode feed supply were conducted during AEMWE operation. From the voltage cycles and electrochemical analyses, eliminating cathode operating feed during cell operation improves the cell performance by 5.8 times with the enhancement in ohmic resistance, activation overpotentials and concentration overpotentials. The optimized binder content in the single-side feed AEMWE operation was determined to be 20 wt.% by varying the PTFE binder content from 5 ~ 20 wt.%. The MEAs fabricated with higher binder content showed higher long-term performance stability while the duration to achieve maximum current density is also extended with increasing binder content. During voltage cycling operation, the high current obtained by changing feed configuration produces gas with higher production rate resulted in reformation of catalyst layer structure. The MEAs with low binder content exhibits high initial performance, but rapid performance degradation is observed from the destruction of pore structures and catalyst loss. The MEAs with sufficient binder content to binds the catalyst under high current operation is required to maintain long-term stability.

Chapter 5. Summary

To fabricate high performance MEAs, the performance degradation mechanisms were studied and the optimized MEA fabrication methods were proposed regarding on the application and operating conditions. In chapter 2, the dry of MEAs during the IT-PEMFC operation was analyzed and the effect of ionomer content in the cathode catalyst layer was investigated. To resolve the dry of MEAs high performance MEAs were fabricated by optimizing cathode catalyst layers. To study the cell performance degradation mechanism in IT-PEMFC, the effect of catalyst layer drying is studied through controlling the low humidified gas flow rate. The ionomer content of cathode catalyst layer is also varied to provide sufficient hydration of ionic conductivity and the influences of drying and flooding is studied under various low relative humidity operating conditions. The introduction of low relative humidified cathode gas significantly affect cell performance and membrane dehydration by removing water from catalyst layer and membrane. By using the water adsorbing property of ionomer, hydration was secured by retaining sufficient ionomer contents for high IT-PEMFC performance. The role of ionomer in providing hydrophilic environment in the catalyst layer further activated in the dry operating conditions of IT-PEMFC. The experimental results indicate that the presence of higher ionomer content in the catalyst layer improves the cell performance, especially under dehydrated conditions. The

ionomer contents of cathode catalyst layer were varied as 20, 30 and 40 wt.% and operated under various low relative humidified gas (10 – 35% RH). MEAs fabricated with 40 wt.% of ionomer content in the cathode catalyst layers exhibited the best performance under the dehydrated operating conditions, such as low-RH inlet gas supply and water production. In chapter 3 and 4, the effect of catalyst layer structures and performance degradation mechanism related to ionic conductivity, reaction kinetics and mass transport of AEMWEs were analyzed under various operating conditions. To produce high performance MEAs of AEMWE, the effects of MEA hot-pressing and binder content in the anode catalyst layer were investigated through electrochemical analyses. Through voltage cycling operation and impedance measurement, the performance influencing factors were determined and the performance degradation mechanisms were analyzed. Pressing the MEAs at 50 ^{o}C improved cell performance by 1.9 times by reducing the polarization resistance (approximately 12%). The ohmic and polarization resistances of MEAs were influenced by binder content in the anode catalyst layer. An insufficient binder loading in the catalyst layer resulted in poor mass transport. Overloading of the binder in the catalyst layer also hinders the electrochemical reaction by covering the electrochemically active surface area of the catalysts and impedes the transport of hydroxide ions and electrons. For the operating condition of supplying H_2O as cathode operating feed, the optimal PTFE binder content was observed with an MEA fabricated with 9 wt.% of binder content in the anode catalyst layer. Through studies of feed configuration the AEMWE cell performance was improved by 5.8 times with reduced ohmic resistances, activation

overpotentials and concentration overpotentials. The elimination of cathode operating feed and supplying KOH solutions to the anode during the cell operation not only improves mass transport of product gas but also activation overpotnetial by higher OH^- ions concentration presented in the cathode through the reactions and back diffused reactants from anode. The high water splitting current during voltage cycle restructures the catalyst layer. The high water splitting current produces large amount of gas. During the process of gas escaping from the catalyst layer, the formation of new paths are expected. The MEAs fabricated with 9 wt.% of binder content in the anode showed high initial cell performance with poor long-term performance stability from destruction of pore structures and catalyst particle loss. On the other hands, the MEAs fabricated with 20 wt.% of binder content in the anode showed high durability. The reformation of catalyst layer structure improves the electrochemically active surface area and mass transport with sufficient binder contents.

The factors influencing cell performances and MEA fabrication method regarding on electrochemical device operating conditions are electrochemically investigated and proposed to provide the further research direction. The electrochemical characteristics observed in this study and the optimization of MEAs are conducted to secure the fundamental techniques to be used for the systems utilized with developed catalysts and ionomer. This study is providing a guide for the research of IT-PEMFC and AEMWE MEAs where only a limited number of studies is reported. Additionally, this study will help to improve further

understanding of degradation mechanisms during the cell operation for fabricating high performance MEAs with extended long-term stability.

References

[1] A.B. Rao, E.S. Rubin, Environmental Science & Technology, 36 (2002) 4467-4475.

[2] W.C. Wang, Y.L. Yung, A.A. Lacis, T. Mo, J.E. Hansen, Science, 194 (1976) 685-690.

[3] M.I. Hoffert, K. Caldeira, G. Benford, D.R. Criswell, C. Green, H. Herzog, A.K. Jain, H.S. Kheshgi, K.S. Lackner, J.S. Lewis, H.D. Lightfoot, W. Manheimer, J.C. Mankins, M.E. Mauel, L.J. Perkins, M.E. Schlesinger, T. Volk, T.M.L. Wigley, Science, 298 (2002) 981-987.

[4] K.R. Smith, M.A.K. Khalil, R.A. Rasmussen, S.A. Thorneloe, F. Manegdeg, M. Apte, Chemosphere, 26 (1993) 479-505.

[5] A. Ahmadi, L. Tiruta-Barna, E. Benetto, F. Capitanescu, A. Marvuglia, Journal of Cleaner Production, 135 (2016) 872-883.

[6] S. Kerdsuwan, K. Laohalidanond, Energy Procedia, 79 (2015) 125-130.

[7] M.J.N. Oliveira Panão, Energy and Buildings, 127 (2016) 736-747.

[8] Z.U. Bayrak, G. Bayrak, M.T. Ozdemir, M.T. Gencoglu, M. Cebeci, International Journal of Hydrogen Energy, 41 (2016) 12569-12581.

[9] S.S. Bhogilla, H. Ito, A. Kato, A. Nakano, Applied Energy, 177 (2016) 309-322.

[10] J. Nowotny, T. Hoshino, J. Dodson, A.J. Atanacio, M. Ionescu, V. Peterson, K.E. Prince, M. Yamawaki, T. Bak, W. Sigmund, T.N. Veziroglu, M.A. Alim, International Journal of Hydrogen Energy, 41 (2016) 12812-12825.

[11] A. Züttel, Mitigation and Adaptation Strategies for Global Change, 12 (2007) 343-365.

[12] K. Christopher, R. Dimitrios, Energy & Environmental Science, 5 (2012) 6640-6651.

[13] C. Song, Catalysis Today, 77 (2002) 17-49.

[14] T. Kreutz, R. Williams, S. Consonni, P. Chiesa, International Journal of Hydrogen Energy, 30 (2005) 769-784.

[15] J.R. Bartels, M.B. Pate, N.K. Olson, International Journal of Hydrogen Energy,

35 (2010) 8371-8384.
[16] D. Barba, F. Giacobbe, A. De Cesaris, A. Farace, G. Iaquaniello, A. Pipino, International Journal of Hydrogen Energy, 33 (2008) 3700-3709.
[17] G. Iaquaniello, F. Giacobbe, B. Morico, S. Cosenza, A. Farace, International Journal of Hydrogen Energy, 33 (2008) 6595-6601.
[18] Y. Kalinci, A. Hepbasli, I. Dincer, International Journal of Hydrogen Energy, 34 (2009) 8799-8817.
[19] B. Coelho, A.C. Oliveira, A. Mendes, Energy & Environmental Science, 3 (2010) 1398-1405.
[20] W. Kreuter, H. Hofmann, International Journal of Hydrogen Energy, 23 (1998) 661-666.
[21] R. O'Hayre, S.-W. Cha, W. Colella, F.B. Prinz, Chapter 1: Introduction, in: Fuel Cell Fundamentals, John Wiley & Sons, Inc, 2016, pp. 1-24.
[22] V.K. Mathur, J. Crawford, Fundamentals of Gas Diffusion Layers in PEM Fuel Cells, in: S. Basu (Ed.) Recent Trends in Fuel Cell Science and Technology, Springer New York, New York, NY, 2007, pp. 116-128.
[23] P.J. Hamilton, B.G. Pollet, Fuel Cells, 10 (2010) 489-509.
[24] S. Asghari, M.H. Shahsamandi, M.R. Ashraf Khorasani, International Journal of Hydrogen Energy, 35 (2010) 9291-9297.
[25] K.H. Lee, S.Y. Lee, D.W. Shin, C. Wang, S.-H. Ahn, K.-J. Lee, M.D. Guiver, Y.M. Lee, Polymer, 55 (2014) 1317-1326.
[26] A. Chandan, M. Hattenberger, A. El-kharouf, S. Du, A. Dhir, V. Self, B.G. Pollet, A. Ingram, W. Bujalski, Journal of Power Sources, 231 (2013) 264-278.
[27] S. Bose, T. Kuila, T.X.H. Nguyen, N.H. Kim, K.-t. Lau, J.H. Lee, Progress in Polymer Science, 36 (2011) 813-843.
[28] S.C. Yeo, A. Eisenberg, Journal of Applied Polymer Science, 21 (1977) 875-898.
[29] A. Stassi, I. Gatto, E. Passalacqua, V. Antonucci, A.S. Arico, L. Merlo, C. Oldani, E. Pagano, Journal of Power Sources, 196 (2011) 8925-8930.
[30] J. Li, M. Pan, H. Tang, RSC Advances, 4 (2014) 3944-3965.

[31] K.D. Kreuer, M. Schuster, B. Obliers, O. Diat, U. Traub, A. Fuchs, U. Klock, S.J. Paddison, J. Maier, Journal of Power Sources, 178 (2008) 499-509.
[32] D.W. Shin, S.Y. Lee, N.R. Kang, K.H. Lee, D.H. Cho, M.J. Lee, Y.M. Lee, K.D. Suh, International Journal of Hydrogen Energy, 39 (2014) 4459-4467.
[33] K. Miyatake, T. Yasuda, M. Watanabe, Journal of Polymer Science Part A: Polymer Chemistry, 46 (2008) 4469-4478.
[34] C. Iojoiu, F. Chabert, M. Maréchal, N.E. Kissi, J. Guindet, J.Y. Sanchez, Journal of Power Sources, 153 (2006) 198-209.
[35] J. Parvole, P. Jannasch, Macromolecules, 41 (2008) 3893-3903.
[36] J.H. Chun, S.G. Kim, J.Y. Lee, D.H. Hyeon, B.-H. Chun, S.H. Kim, K.T. Park, Renewable Energy, 51 (2013) 22-28.
[37] Y. Devrim, S. Erkan, N. Baç, I. Eroğlu, International Journal of Hydrogen Energy, 34 (2009) 3467-3475.
[38] K.T. Park, S.G. Kim, J.H. Chun, D.H. Jo, B.-H. Chun, W.I. Jang, G.B. Kang, S.H. Kim, K.B. Lee, International Journal of Hydrogen Energy, 36 (2011) 10891-10900.
[39] G. Gnana Kumar, A.R. Kim, K. Suk Nahm, R. Elizabeth, International Journal of Hydrogen Energy, 34 (2009) 9788-9794.
[40] C. Kunusch, P. Puleston, M. Mayosky, Sliding-Mode Control of PEM Fuel Cells, Springer-Verlag London London, UK, 2012.
[41] E. Passalacqua, F. Lufrano, G. Squadrito, A. Patti, L. Giorgi, Electrochimica Acta, 46 (2001) 799-805.
[42] G. Sasikumar, J.W. Ihm, H. Ryu, Journal of Power Sources, 132 (2004) 11-17.
[43] S. Jeon, J. Lee, G.M. Rios, H.-J. Kim, S.-Y. Lee, E. Cho, T.-H. Lim, J. Hyun Jang, International Journal of Hydrogen Energy, 35 (2010) 9678-9686.
[44] K.-H. Kim, K.-Y. Lee, H.-J. Kim, E. Cho, S.-Y. Lee, T.-H. Lim, S.P. Yoon, I.C. Hwang, J.H. Jang, International Journal of Hydrogen Energy, 35 (2010) 2119-2126.
[45] S. Kamarajugadda, S. Mazumder, Journal of Power Sources, 183 (2008) 629-642.
[46] K.-H. Kim, K.-Y. Lee, S.-Y. Lee, E. Cho, T.-H. Lim, H.-J. Kim, S.P. Yoon, S.H.

Kim, T.W. Lim, J.H. Jang, International Journal of Hydrogen Energy, 35 (2010) 13104-13110.
[47] B.-S. Lee, S.H. Ahn, H.-Y. Park, I. Choi, S.J. Yoo, H.-J. Kim, D. Henkensmeier, J.Y. Kim, S. Park, S.W. Nam, K.-Y. Lee, J.H. Jang, Applied Catalysis B: Environmental, 179 (2015) 285-291.
[48] D.S. Hwang, C.H. Park, S.C. Yi, Y.M. Lee, International Journal of Hydrogen Energy, 36 (2011) 9876-9885.
[49] Y. Qiu, H. Zhang, H. Zhong, F. Zhang, International Journal of Hydrogen Energy, 38 (2013) 5836-5844.
[50] T. Suzuki, S. Tsushima, S. Hirai, International Journal of Hydrogen Energy, 36 (2011) 12361-12369.
[51] J.W. Lim, Y.H. Cho, M. Ahn, D.Y. Chung, Y.H. Cho, N. Jung, Y.S. Kang, O.H. Kim, M.J. Lee, M. Kim, Y.E. Sung, Journal of the Electrochemical Society, 159 (2012) B378-B384.
[52] S. Litster, G. McLean, Journal of Power Sources, 130 (2004) 61-76.
[53] S. Holdcroft, Chemistry of Materials, 26 (2013) 381-393.
[54] A.S. Aricò, S. Siracusano, N. Briguglio, V. Baglio, A. Di Blasi, V. Antonucci, Journal of Applied Electrochemistry, 43 (2013) 107-118.
[55] Y. Leng, G. Chen, A.J. Mendoza, T.B. Tighe, M.A. Hickner, C.-Y. Wang, Journal of the American Chemical Society, 134 (2012) 9054-9057.
[56] P. Millet, F. Andolfatto, R. Durand, International Journal of Hydrogen Energy, 21 (1996) 87-93.
[57] A. Goñi-Urtiaga, D. Presvytes, K. Scott, International Journal of Hydrogen Energy, 37 (2012) 3358-3372.
[58] T. Morimoto, M. Yoshitake, S. Morikawa, Y. Oda, International Journal of Hydrogen Energy, 11 (1986) 503-506.
[59] M. Carmo, D.L. Fritz, J. Mergel, D. Stolten, International Journal of Hydrogen Energy, 38 (2013) 4901-4934.
[60] J. Parrondo, C.G. Arges, M. Niedzwiecki, E.B. Anderson, K.E. Ayers, V. Ramani, RSC Advances, 4 (2014) 9875-9879.

[61] S.H. Lee, J.C. Rasaiah, The Journal of Chemical Physics, 135 (2011) 124505.
[62] S. Zhang, C. Li, X. Xie, F. Zhang, International Journal of Hydrogen Energy, 39 (2014) 13718-13724.
[63] N. Yokota, M. Shimada, H. Ono, R. Akiyama, E. Nishino, K. Asazawa, J. Miyake, M. Watanabe, K. Miyatake, Macromolecules, 47 (2014) 8238-8246.
[64] Y.-C. Cao, X. Wu, K. Scott, International Journal of Hydrogen Energy, 37 (2012) 9524-9528.
[65] M. Faraj, M. Boccia, H. Miller, F. Martini, S. Borsacchi, M. Geppi, A. Pucci, International Journal of Hydrogen Energy, 37 (2012) 14992-15002.
[66] Y. Liu, B. Zhang, C.L. Kinsinger, Y. Yang, S. Seifert, Y. Yan, C. Mark Maupin, M.W. Liberatore, A.M. Herring, Journal of Membrane Science, 506 (2016) 50-59.
[67] D. Aili, M.K. Hansen, R.F. Renzaho, Q. Li, E. Christensen, J.O. Jensen, N.J. Bjerrum, Journal of Membrane Science, 447 (2013) 424-432.
[68] L.A. Diaz, J. Hnát, N. Heredia, M.M. Bruno, F.A. Viva, M. Paidar, H.R. Corti, K. Bouzek, G.C. Abuin, Journal of Power Sources, 312 (2016) 128-136.
[69] J. Fang, Y. Yang, X. Lu, M. Ye, W. Li, Y. Zhang, International Journal of Hydrogen Energy, 37 (2012) 594-602.
[70] S.A. Nuñez, M.A. Hickner, ACS Macro Letters, 2 (2013) 49-52.
[71] O.D. Thomas, K.J.W.Y. Soo, T.J. Peckham, M.P. Kulkarni, S. Holdcroft, Journal of the American Chemical Society, 134 (2012) 10753-10756.
[72] A.G. Wright, S. Holdcroft, ACS Macro Letters, 3 (2014) 444-447.
[73] D. Henkensmeier, H. Cho, M. Brela, A. Michalak, A. Dyck, W. Germer, N.M.H. Duong, J.H. Jang, H.-J. Kim, N.-S. Woo, T.-H. Lim, International Journal of Hydrogen Energy, 39 (2014) 2842-2853.
[74] G. Wang, Y. Weng, D. Chu, R. Chen, D. Xie, Journal of Membrane Science, 332 (2009) 63-68.
[75] T.J. Clark, N.J. Robertson, H.A. Kostalik Iv, E.B. Lobkovsky, P.F. Mutolo, H.D. Abruña, G.W. Coates, Journal of the American Chemical Society, 131 (2009) 12888-12889.
[76] G. Wang, Y. Weng, J. Zhao, D. Chu, D. Xie, R. Chen, Polymers for Advanced

Technologies, 21 (2010) 554-560.
[77] H.A. Kostalik, T.J. Clark, N.J. Robertson, P.F. Mutolo, J.M. Longo, H.D. Abruña, G.W. Coates, Macromolecules, 43 (2010) 7147-7150.
[78] S. Seetharaman, R. Balaji, K. Ramya, K.S. Dhathathreyan, M. Velan, International Journal of Hydrogen Energy, 38 (2013) 14934-14942.
[79] X. Wu, K. Scott, Journal of Materials Chemistry, 21 (2011) 12344-12351.
[80] X. Wu, K. Scott, International Journal of Hydrogen Energy, 38 (2013) 3123-3129.
[81] D. Strmcnik, M. Uchimura, C. Wang, R. Subbaraman, N. Danilovic, V. van der, A.P. Paulikas, V.R. Stamenkovic, N.M. Markovic, Nat Chem, 5 (2013) 300-306.
[82] K. Artyushkova, D. Habel-Rodriguez, T.S. Olson, P. Atanassov, Journal of Power Sources, 226 (2013) 112-121.
[83] W.R.W. Daud, A.B. Mohamad, A.A.H. Kadhum, R. Chebbi, S.E. Iyuke, Energy Conversion and Management, 45 (2004) 3239-3249.
[84] C. Suo, X. Liu, X. Tang, Y. Zhang, B. Zhang, P. Zhang, Electrochemistry Communications, 10 (2008) 1606-1609.
[85] S. Towne, V. Viswanathan, J. Holbery, P. Rieke, Journal of Power Sources, 171 (2007) 575-584.
[86] F. Mack, T. Morawietz, R. Hiesgen, D. Kramer, V. Gogel, R. Zeis, International Journal of Hydrogen Energy, 41 (2016) 7475-7483.
[87] C.C. Pavel, F. Cecconi, C. Emiliani, S. Santiccioli, A. Scaffidi, S. Catanorchi, M. Comotti, Angewandte Chemie International Edition, 53 (2014) 1378-1381.
[88] L. Zeng, T.S. Zhao, Nano Energy, 11 (2015) 110-118.
[89] S.H. Ahn, B.-S. Lee, I. Choi, S.J. Yoo, H.-J. Kim, E. Cho, D. Henkensmeier, S.W. Nam, S.-K. Kim, J.H. Jang, Applied Catalysis B: Environmental, 154–155 (2014) 197-205.
[90] C.M. Pedersen, M. Escudero-Escribano, A. Velázquez-Palenzuela, L.H. Christensen, I. Chorkendorff, I.E.L. Stephens, Electrochimica Acta, 179 (2015) 647-657.
[91] Y. Song, Y. Wei, H. Xu, M. Williams, Y. Liu, L.J. Bonville, H. Russell Kunz,

J.M. Fenton, Journal of Power Sources, 141 (2005) 250-257.
[92] M.-J. Choo, K.-H. Oh, H.-T. Kim, J.-K. Park, ChemSusChem, 7 (2014) 2335-2341.
[93] Y. Song, H. Xu, Y. Wei, H.R. Kunz, L.J. Bonville, J.M. Fenton, Journal of Power Sources, 154 (2006) 138-144.
[94] I. Gatto, A. Stassi, V. Baglio, A. Carbone, E. Passalacqua, A.S. Aricò, M. Schuster, B. Bauer, Electrochimica Acta, 165 (2015) 450-455.
[95] H. Xu, H.R. Kunz, J.M. Fenton, Electrochimica Acta, 52 (2007) 3525-3533.
[96] C.-C. Ke, X.-J. Li, Q. Shen, S.-G. Qu, Z.-G. Shao, B.-L. Yi, International Journal of Hydrogen Energy, 36 (2011) 3606-3613.
[97] A. Guimet, L. Chikh, A. Morin, O. Fichet, Journal of Membrane Science, 514 (2016) 358-365.
[98] D. Gerteisen, N. Zamel, C. Sadeler, F. Geiger, V. Ludwig, C. Hebling, International Journal of Hydrogen Energy, 37 (2012) 7736-7744.
[99] F.-B. Weng, A. Su, C.-Y. Hsu, International Journal of Hydrogen Energy, 32 (2007) 666-676.
[100] M. Ji, Z. Wei, Energies, 2 (2009) 1057.
[101] C. Lei, D. Bessarabov, S. Ye, Z. Xie, S. Holdcroft, T. Navessin, Journal of Power Sources, 196 (2011) 6168-6176.
[102] Z. Xie, X. Zhao, J. Gazzarri, Q. Wang, T. Navessin, S. Holdcroft, ECS Transactions, 25 (2009) 1187-1192.
[103] M.J. Cheah, I.G. Kevrekidis, J. Benziger, The Journal of Physical Chemistry B, 115 (2011) 10239-10250.
[104] Q. Li, R. He, J.O. Jensen, N.J. Bjerrum, Chemistry of Materials, 15 (2003) 4896-4915.
[105] S.E. Iyuke, A.B. Mohamad, A.A.H. Kadhum, W.R.W. Daud, C. Rachid, Journal of Power Sources, 114 (2003) 195-202.
[106] S. Gamburzev, A.J. Appleby, Journal of Power Sources, 107 (2002) 5-12.
[107] Y. Jeon, J.-I. Park, J. Ok, A. Dorjgotov, H.-J. Kim, H. Kim, C. Lee, S. Park, Y.-G. Shul, International Journal of Hydrogen Energy, 41 (2016) 6864-6876.

[108] J. Lobato, H. Zamora, J. Plaza, P. Cañizares, M.A. Rodrigo, Applied Catalysis B: Environmental, 198 (2016) 516-524.
[109] S.M. Andersen, R. Dhiman, M.J. Larsen, E. Skou, Applied Catalysis B: Environmental, 172–173 (2015) 82-90.
[110] A. Therdthianwong, P. Manomayidthikarn, S. Therdthianwong, Energy, 32 (2007) 2401-2411.
[111] Y. Sone, P. Ekdunge, D. Simonsson, Journal of The Electrochemical Society, 143 (1996) 1254-1259.
[112] C.Y. Chen, C.S. Tsao, International Journal of Hydrogen Energy, 31 (2006) 391-398.
[113] R. Lin, T. Zhao, H. Zhang, C. Cao, B. Li, J. Ma, Chinese Journal of Mechanical Engineering, 25 (2012) 1171-1175.
[114] R. Mosdale, M. Wakizoe, S. Srinivasan, Electrochemical Society, Pennington, NJ, 1994.
[115] W. Song, H. Yu, L. Hao, Z. Miao, B. Yi, Z. Shao, Solid State Ionics, 181 (2010) 453-458.
[116] G.S. Avcioglu, B. Ficicilar, I. Eroglu, International Journal of Hydrogen Energy, 41 (2016) 10010-10020.
[117] G. Jeong, M. Kim, J. Han, H.-J. Kim, Y.-G. Shul, E. Cho, Journal of Power Sources, 323 (2016) 142-146.
[118] S. Kim, T.D. Myles, H.R. Kunz, D. Kwak, Y. Wang, R. Maric, Electrochimica Acta, 177 (2015) 190-200.
[119] Y.S. Li, T.S. Zhao, Z.X. Liang, Journal of Power Sources, 190 (2009) 223-229.
[120] S.H. Ahn, S.J. Yoo, H.-J. Kim, D. Henkensmeier, S.W. Nam, S.-K. Kim, J.H. Jang, Applied Catalysis B: Environmental, 180 (2016) 674-679.
[121] V. Radhakrishnan, P. Haridoss, International Journal of Hydrogen Energy, 36 (2011) 14823-14828.
[122] H.-K. Lee, J.-H. Park, D.-Y. Kim, T.-H. Lee, Journal of Power Sources, 131 (2004) 200-206.

[123] J.-C. Lin, C.-M. Lai, F.-P. Ting, S.-D. Chyou, K.-L. Hsueh, Journal of Applied Electrochemistry, 39 (2009) 1067-1073.
[124] V.B. Silva, A. Rouboa, Journal of Electroanalytical Chemistry, 671 (2012) 58-66.
[125] I. Dedigama, P. Angeli, K. Ayers, J.B. Robinson, P.R. Shearing, D. Tsaoulidis, D.J.L. Brett, International Journal of Hydrogen Energy, 39 (2014) 4468-4482.
[126] H. Meng, C.-Y. Wang, Journal of The Electrochemical Society, 151 (2004) A358-A367.
[127] J. Zhang, G.-P. Yin, Z.-B. Wang, Q.-Z. Lai, K.-D. Cai, Journal of Power Sources, 165 (2007) 73-81.
[128] B. Bladegroem, H. Su, S. Pasupathi, V. Linkov, Electrolysis, in: V. Linkov (Ed.) Overview of Membrane Electrode Assembly Preparation Methods for Solid Polyemr Electrolyte Electrolyzer, InTech, 2012, pp. 290.
[129] L. Xiao, S. Zhang, J. Pan, C. Yang, M. He, L. Zhuang, J. Lu, Energy & Environmental Science, 5 (2012) 7869-7871.
[130] J. Parrondo, M. George, C. Capuano, K.E. Ayers, V. Ramani, Journal of Materials Chemistry A, 3 (2015) 10819-10828.
[131] A.D. James Larminie, Fuel cell systems explained, 2nd ed., Wiley, England, 2000.

Appendix A. Publications derived from electrochemistry work

Chapter 2

Min Kyung Cho, Hee-Young Park, So Young Lee, Byung-Seok Lee, Hyoung-Juhn Kim, Dirk Henkensmeier, Sung Jong Yoo, Jin Young Kim, Jonghee Han, Hyun S. Park, Yung-Eun Sung, Jong Hyun Jang, " Effect of Catalyst Layer Ionomer Content on Performance of Intermediate Temperature Proton Exchange Membrane Fuel Cells (IT-PEMFCs) under Reduced Humidity Conditions", *In Press, Accepted to Electrochimica Acta.*

Chapter 3

Min Kyung Cho, Hee-Young Park, Seunghoe Choe, Sung Jong Yoo, Jin Young Kim, Hyoung-Juhn Kim, Dirk Henkensmeier, So Young Lee, Yung-Eun Sung, Hyun S. Park, Jong Hyun Jang, "Factors in Catalyst Layer Fabrication for Enhanced Performance in Anion Exchange Membrane Water Electrolysis", *Under revision, Submitted to Journal of Power sources.*

Chapter 4

Min Kyung Cho, Hee-Young Park, Seunghoe Choe, Sung Jong Yoo, Jin Young Kim, Hyoung-Juhn Kim, Dirk Henkensmeier, So Young Lee, Yung-Eun Sung, Hyun S. Park, Jong Hyun Jang, "Factors in Catalyst Layer Fabrication for Enhanced Performance in Anion Exchange Membrane Water

Electrolysis", *In preparation, expected submission in January 2017.*

Other works

Byung-Seok Lee, Hee-Young Park, **Min Kyung Cho**, Jae Woo Jung, Hyoung-Juhn Kim, Dirk Henkensmeier, Sung Jong Yoo, Jin Young Kim, Sehkyu Park, Kwang-Young Lee, Jong Hyun Jang, "Development of porous Pt/IrO_2/carbon paper electrocatalysts with enhanced mass transport as oxygen electrodes in unitized regenerative fuel cells", *Electrochemistry Comunications 64 (2016) 14-17.*

Byung-Seok Lee, Hee-Young Park, Insoo Choi, **Min Kyung Cho**, Hyoung-Juhn Kim, Sung Jong Yoo, Dirk Henkensmeier, Jin Young Kim, Suk Woo Nam, Sehkyu Park, Kwang-Young Lee, Jong Hyun Jang, "Polarization characteristics of a low catalyst loading PEM water electrolyzer operating at elevated temperature", *Journal of Power Sources 309 (2016) 127-134.*

Min Kyung Cho, Dae-Nyung Lee, Yi-Young Kim, Jonghee Han, Hyoung-Juhn Kim, EunAe Cho, Tae-Hoon Lim, Dirk Henkensmeier, Sung Jong Yoo, Young-Eun Sung, Sehkyu Park, Jong Hyun Jang, "Analysis of the spatially distributed performance degradation of a polymer electrolyte membrane fuel cell stack", *International Journal of Hydrogen Energy 39 (2014) 16548-16555.*

국 문 초 록

중온 양이온 교환막 연료전지와 알칼리 음이온 교환막 수전해 장치용 막-전극 접합체 연구

대체 에너지 자원으로서 수소 에너지에대한 관심이 증가 함에 따라 수소를 연료로 이용하여 전기를 발생시키거나 물을 이용하여 수소를 발생시키는 전기화학변환 장치에 대한 연구가 활발히 진행 되고 있다. 양이온 교환 막 연료전지는 고분자 전해질 막을 양이온 전도체로 이용하며 고분자 전해질 막 연료전지로도 불린다. 이 연료전지는 수소와 산소를 전기와 물로 변환 시키는 전기화학적 장치이다. 양이온 교환 막 연료전지의 큰 이점은 기존 내연기관 (20-30%) 보다 높은 열역학적 효율 (> 40%)과 더불어 운전 중 온실가스 발생이 없다는 것이다. 수소 생산부터 전기변환 까지 청정 시스템을 이루기 위해, 물 전기 분해와 연료전지 기술 개발을 위한 집중 적인 연구가 이루어 지고 있다.

중온 양이온 교환막 연료전지는 양이온 교환막 저온 연료전지 (~ 80 ºC) 에 비해 높은 온도 (100–120 °C) 에서 운전 된다. 증가된 시스템의 구동 온도를 통하여 반응 속도와 일산화탄소 피독에 대한 내성 향상 및 열/물 관리가 용이해지는 장점을 얻을 수 있다. 그러므로, 중온 양이온 교환막 연료전지는 저온 양이온 교환막 연료전지에 비교하여 많은 장점들이 예상된다. 알칼리 전해용액과 다공성의 다이아프램 분리막을 이용하는 기존의 알칼리 수전해 기술과 비교하여 알칼리 음이온 교환막 수전해의 경우 많은 장점을 가지고 있다. 고분자 막 기반의 시스템을 이용함으로써 안전성, 효율성과 발생기체의 분리가 향상된다. 그에 더불어, 양이온 교환막 수전해 시스템과 다르게 특징적인 알칼리 운전 조건은 산소와 수소 발생 전극에 저렴한 비귀금속 촉매 사용을 가능하게 하였다. 이런 큰 장점들에도 불구하고 운전 특성으로 인하여 중온 양이온 교환막 연료전지나 알칼리 음이온 교환막 수전해는 저온 양이온 교환막 연료전지나 양이온 교환막 수전해에 비해 낮은 성능을 보이고 있다.

연구들은 대부분 재료 개발 위주로 진행 되고 있다. 개발된 고분자 막과 촉매들의 뛰어난 재료 특성에도 불구하고 단위 전지 성능에는 잘 반영이 되지 않고 있다. 단위 전지는 고분자 막을 기준으로 양면에 촉매층으로 이루어진 막-전극 접합체를 포함하고 있다. 촉매와 바인더로 구성된 촉매층은 전기화학 반응및 반응물과 생성물의 물질

전달이 이루어 지기 때문에 막-전극 접합체에서 매우 중요한 구성요소이다. 그러므로, 전기화학소자의 구동 조건에 따라 고성능과 고내구성을 이루기 위해 촉매층의 구조와 특성의 최적화를 필요로 한다. 촉매층 내의 이온전도와 물질 전달은 촉매위에 형성된 이오노머 필름에 의존되기 때문에 중온 양이온 교환막 연료전지의 막-전극 접합체의 건조현상이 단위전지 성능에 주된 영향을 준다. 중온 양이온 교환막 연료전지 연구에서는 120 ºC, 35% 이하의 가습 운전 조건에서 막-전극 접합체의 건조현상을 실험적으로 증명 하였고 고성능을 위한 효과적인 촉매층 형성을 위하여 흡습 능력이 있는 이오노머 함량을 20 에서 40 wt.%까지 제어해 보았다. 단위 전지 성능은 전류 밀도 감소에 따라 막-전극 접합체의 건조현상이 홍수 현상보다 더 우세한 영향을 주게되고 그에 따라 최적 이오노머의 함량이 증가되는 경향을 보였다. 그러나, 물의 발생속도가 높고 충분한 수화가 충족되는 고전류 밀도에서는 홍수 현상으로 인하여 30wt.% 이오노머 함량에서 최고 성능을 얻을 수 있었다. 알칼리 음이온 교환막 수전해의 경우 막-전극 접합체의 프레스와 피드 공급 조건에 따른 영향에 대한 연구가 진행 되었다. 프레스 공정을 도입 함으로써 물질 전달 향상을 통한 수전해 전류밀도 증가를 확인 하였다. 추가 적으로, 반응 용액이 애노드와 캐소드 모두에 공급이 되는 더블사이드 피드의 특성과 애노드 쪽에만 반응물이 공급되는 싱글사이드 피드의 특성이 다양한 애노드 바인드 함량에서

연구 되었다. 더블사이드 운전의 경우 전지 성능은 촉매의 전기화학 활성 면적과 촉매층의 기공구조에 지배적인 영향을 받는 것을 밝혀 내었다. 5 에서 20 wt.% 까지 바인더 함량을 변화 시킨 결과 9 wt.% 의 바인더 함량에서 최적 함량을 얻을 수 있었다. 싱글사이드 운전의 경우 높은 전류 밀도 운전에서는 다량의 산소가 발생되고 이는 촉매 유실을 일으켜 심각한 장기 성능 문제가 발생 되는 것을 발견 하였다. 그러므로, 이 실험에서 바인더 함량이 가장 많았던 20 wt.% 에서 최고의 내구성과 단위전지 성능이 얻어졌다. 본 연구에서는 운전 방법에 따른 전기소자의 단위전지 성능에 영향을 미치는 전기화학적 주요 요인을 분석 하였고 고성능 발현을 위한 막-전극 접합체 연구 방향을 제시 하였다.

주요어 : 막-전극 접합체, 바인더 함량, 중온 양이온 교환막 연료전지, 알칼리 음이온 교환막 수전해, 전기화학

학 번 : 2012-31302